

Generation of Realistic Cloud Access Times for Mobile Application Testing using Transfer Learning

1st Manoj R. Rege
Technische Universität Berlin
Berlin, Germany
manojrege@mailbox.tu-berlin.de

2nd Vlado Handziski
R3 Reliable Realtime Radio
Berlin, Germany
vlado.handziski@r3coms.com

3rd Adam Wolisz
Technische Universität Berlin
Berlin, Germany
wolisz@tkn.tu-berlin.de

Abstract—The network Quality of Service (QoS) metrics such as the access time, the bandwidth, and the packet loss play an important role in determining the Quality of Experience (QoE) of mobile applications. Various factors like the Radio Resource Control (RRC) states, the Mobile Network Operator (MNO) specific retransmission configurations, handovers triggered by the user mobility, the network load, etc. can cause high variability in these QoS metrics on 4G/LTE, and WiFi networks, which can be detrimental to the application QoE. Therefore, exposing the mobile application to realistic network QoS metrics is critical for a tester attempting to predict its QoE. A viable approach is testing using synthetic traces. The main challenge in the generation of realistic synthetic traces is the diversity of environments and the lack of wide scope of real traces to calibrate the generators. In this paper, we describe a measurement-driven methodology based on transfer learning with Long Short Term Memory (LSTM) neural nets to solve this problem. The methodology requires a relatively short sample of the targeted environment to adapt the presented basic model to new environments, thus simplifying synthetic traces generation. We present this feature for realistic WiFi and LTE cloud access time models adapted for diverse target environments with a trace size of just 6000 samples measured over a few tens of minutes. We demonstrate that synthetic traces generated from these models are capable of accurately reproducing application QoE metric distributions including their outlier values.

Index Terms—Mobile, Cloud, Network, Access Time, Transfer Learning, Long Short Term Memory, Neural Net, Testing

I. INTRODUCTION

The Quality of Experience (QoE) of mobile applications is highly dependent on factors such as the access network Quality of Service (QoS), and the user context, among others. It has been observed that in the widely deployed cellular networks like 3G, 4G/LTE, and WiFi, various problems in the network stack can cause significant variability in the network QoS metrics such as the access time latency, bandwidth, packet loss, etc. Such high variability can have an adverse impact on the mobile application QoE [1]–[8]. For example, when using a cellular network like LTE, Radio Resource Control (RRC) radio link layer control states which are used by the base station to coordinate with the device have a significant impact on application performance and power consumption [1], [2]. On the data plane, Mobile Network Operators (MNOs) often

employ protocols configurations in the Radio Link Control (RLC) that can adversely impact the performance of transport protocols like TCP, thus degrading the application QoE [3]. External user context factors like mobility lead to handover within the network that can introduce large access time latencies and degrade application throughput [4]. When a large number of cell users are connected to the network, there can be RRC failures for new users either blocking their network access or increasing the connection establishment latency [5]. At certain times of the day, overall higher demand for video-streaming, web applications can increase the aggregate network traffic volume in the downlink, thereby degrading the throughput and the access time latency which is detrimental to application QoE [6]. With the wide-scale roll-out of the 5G networks, some of these problems could fade away. Also, the situation might ease out if the slices supporting the stable network QoS and those matching the individual application requirements will be rolled out. But the scope of availability of such application-specific slices in the near future is not quite clear.

Continuous measurement of application QoE and its improvement has a strong incentive for the application testers, as it is essential for the business's success. The application testers require a good understanding of the network QoS delivered to the users in the real world. This can help them to fine-tune application-specific protocols and parameters to improve their QoE. For example, in video streaming based applications the buffer sizes and streaming rates need to be fine-tuned based on the network QoS [9]. We argue that there is a common need across the various application use-cases to study the impact of network QoS on the application QoE in a given context which is limited to specific scope of interest. For instance, measuring QoE in a variety of scenarios such as users physical environment viz. indoors, outdoors, in a cafe, or a university, etc, within a metropolitan region, while the user is mobile; commuting, driving a vehicle, etc., during certain hours of the day, on a specific MNO, on a specific mobile device model, or any other such factors that impact the network QoS and thus the application QoE. We refer to such narrow scope of QoE testing as target environment context-driven testing. In this work, we focus on target environment context-driven testing under the impact of cloud access time network QoS metric as it has the strongest influence on the perceived overall QoE

This work has been partially supported by the German Federal Ministry of Education and Research (BMBF) within the project SecureFog under the grant number 16KIS0777.

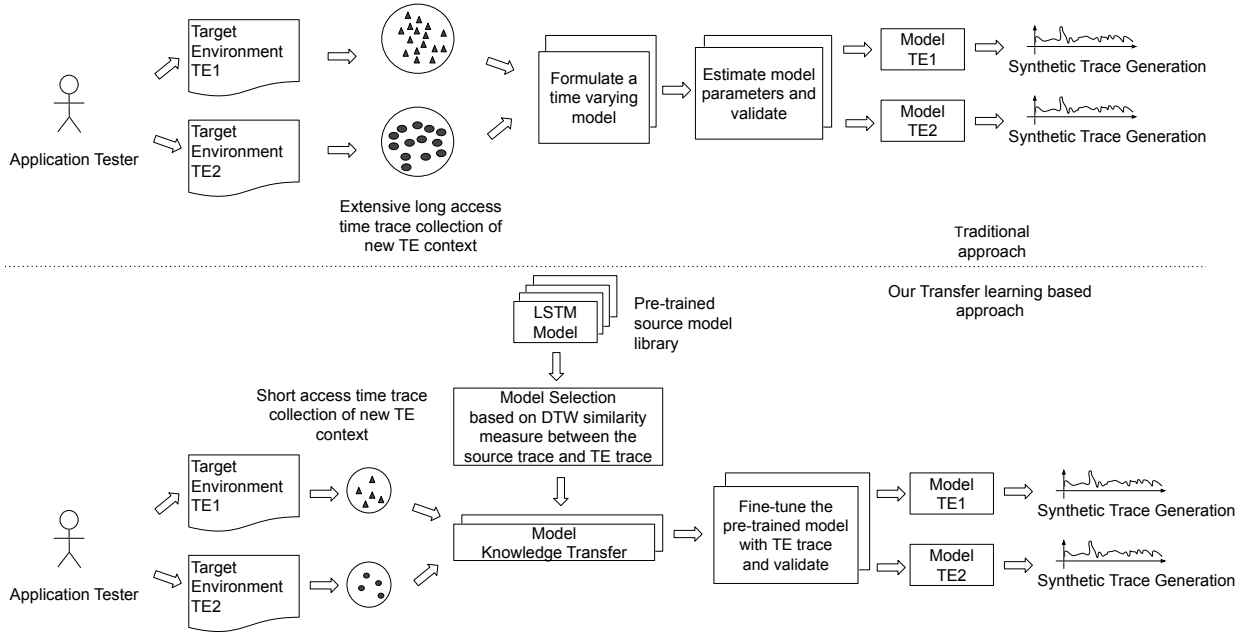


Fig. 1: Cloud access time modeling: A comparison of our transfer learning based approach with the traditional approach.

for numerous mobile applications. Amazon [10] estimates that an increase of access time latency by 100 ms can lead to 1% annual sales loss. A similar study from Google [11] has found that 500 ms latency per transaction can result in loss of traffic as high as 20%.

Unfortunately, the current approach for QoE testing is not suited for carrying out target environment context-driven testing. It typically makes use of a strongly oversimplified access time model represented by the mean and standard deviation statistics of the well-known parametric distributions [12]. These statistics are either derived through common knowledge or from the literature. Such an approach has fundamental shortcomings. Firstly, the access time statistics obtained from literature, databases [13] do not include the temporal dynamics of the access time variations; hence they lack realism. Secondly, these statistics are often generic, labeled by location and access network type — WiFi, 3G, and LTE. They lack context-based labels related to the trace collection environment such as stationary, mobility, indoors, outdoors, etc. Joorabchi et al. [14] in their survey-based study of mobile application developers and testers found the lack of support to accurately mimic realistic network environments as one of the top challenges in mobile application development and testing.

According to [15], [16], there are three main approaches for carrying out more rigorous application testing viz. real, emulation, and simulation models. The real approach includes exposing the application on a real mobile device to real network conditions directly. While this approach seems to have the highest level of realism, it is hard to cover a large enough scope of conditions. Furthermore, the real network conditions cannot be controlled and testing is not repeatable.

An alternative is to build a comprehensive trace archive that contains cloud access time traces and replay them to emulate real network conditions [17]. While the trace-based emulation approach is valuable, such open archives are not available. Further, it is also likely that any such archive would have to be continuously updated given the high variability of target environments and contexts. The simulation modeling approach includes building a model for generating synthetic cloud access time traces that mimic a large scope of real-world conditions in a controllable and statistically repeatable way. Models have the potential to be representative of the broader population of users and scenarios if they properly interpolate and extrapolate the set of measurements used for its creation. Unfortunately, models might also need frequent re-calibration if the environment changes.

Building good models is non-trivial. The traditional modeling approach (shown in Figure 1) requires an extensive long collection of traces for a representative set of target environments. According to [18], trace collection for network modeling requires careful consideration of parameter values for granularity, duration, scale, diversity of measurement points for traces. Next, the traces need to be processed and then reduced to parameters of a time-varying model [15]. Thereafter, the parameters of the model need to be estimated and the model validated. For a newer target environment, the entire set of steps need to be repeated again. Thus, building models is hardly a feasible approach for a tester of a single application or a small number of applications. Most application testers are not networking experts and lack of sufficient domain knowledge makes both data collection and building such models challenging for them. Therefore, the rigorous network

modeling approach has been of limited interest within the application testing community in industry [19].

This paper aims to lower the barriers to building realistic cloud access time models for the generation of synthetic traces that can be used in target environment context-driven testing. We develop a transfer learning based approach to build a model for a target environment (shown in Figure 1). We claim and demonstrate that our approach requires a relatively short measurement trace of cloud access time within a target environment to build its realistic model as compared to traditional approaches to model realistic cloud access times [20], [21] that require extensively long targeted environment traces. We build a library of so-called source models by training a Long Short Term Memory (LSTM) neural net architecture on an extensive set of traces of cloud access times collected over WiFi as well as LTE networks in various contexts. These contexts include scenarios such as indoor, and outdoor environments, stationary, and mobility in the train, vehicle, and walking. Then to build the model of a newer target environment, an appropriate pre-trained model is selected from the library based on the Dynamic Time Warping (DTW) similarity measure between the source and the target traces. The learned features (the net's weights) of the selected pre-trained model are then transferred in the lower layers of the selected pre-trained source model by freezing them, also called knowledge transfer. Finally, the model is fine-tuned by training on the higher layers with the target environment trace and then validated. The main challenges in applying transfer learning to the trace generation problem are summarized by the following open questions. (1) Which pre-trained source model to select as the source for the knowledge transfer? (2) How much knowledge to transfer? (3) How much target environment trace will be sufficient for fine-tuning to generate realistic traces? In this paper, we pursue a systematic investigation to answer these questions.

The main contributions of our work are as follows:

- Source model generation
 - We propose a generic LSTM neural net architecture for modeling cloud access times that is instantiable across any target environment.
 - We have built an access time trace archive spanning across target environments that include user mobility (vehicle, train, walk), a stationary user at different locations (cafe, dormitory, university campus, home, office) on WiFi and LTE networks.
 - Through systematic training and validation, we instantiate the LSTM architecture for each of these environment traces in the archive, thus resulting in a library of 10 pre-trained LSTM source models. This library of source models can be extended as needs appear.
- Target model development
 - Our simplified library of pre-trained source models covering a spectrum of useful environments can be directly used for obtaining models of the newer target environments through fine-tuning on its short sample trace. This eliminates the need for tedious long trace

collection.

- We suggest how to select the source model for a given target environment using the similarity measure like Dynamic Time Warping (DTW) and demonstrate the usefulness of such selection.
- Using the Symmetrical Mean Absolute Percentage Error (SMAPE) as the model performance metric, we find that more knowledge transfer in terms of an increased number of transferred layers does not necessarily mean higher accuracy.
- We assess the impact of the amount of target trace on the accuracy of the fine-tuned model, giving recommendations to this point.
- *ContextPerf* automation tool
 - We automate the process of selecting a pre-trained source model, fine-tuning the model using the target environment trace, and generating synthetic traces using the fine-tuned model by prototyping a tool called *ContextPerf*.
- Real mobile application QoE testing
 - We carry out example testing case-studies to estimate QoE metrics of *Instagram* and *Conversations* chat messenger mobile applications. The case-studies compare the QoE metric distributions obtained by using our synthetic access time traces with those obtained using the popular and simple normally distributed access time model.

The paper is organized as follows: Cloud access time impact on various categories of mobile application QoE is discussed in Section II. Section III introduces the problem of modeling cloud access times using LSTMs and transfer learning. Section IV and Section V present the details of our methodology and performance analysis of transfer learning to build cloud access time models. The synthetic traces generated using the model are integrated with the mobile network emulator in Section VI. Section VII describes mobile application testing case-studies to measure QoE of two popular mobile applications using synthetic traces. The related work is discussed in Section VIII. Discussion of future work and challenges is presented in Section IX. Finally, we conclude in Section X.

II. CLOUD ACCESS TIMES AND THE MOBILE APPLICATION QOE

In this section, we discuss the quantified impact of cloud access times on the QoE for various categories of mobile applications. Access time is measured as the time duration starting from when the first packet is sent by the application task to the time when it reaches the destination cloud backend and vice versa from the cloud backend to the application task. The interaction of an application task with the cloud backend spans over multiple flows. Therefore, response times become additive and can accumulate. A slight increase in single access flow latency can significantly impact the response time of the application, thus adversely impacting the overall application QoE.

The severity of the impact depends on the application category and the action tasks within them. For mobile web-

based applications, Page Load Time (PLT) is one of the most important QoE metrics. The changes in cloud access times impact PLTs. According to the study in [22], a 25% reduction in the access time reduces the PLT by 45%. Another study by Belshe [23] shows that every 20 ms decrease in access time leads to a linear decrease in the PLT. When the access times are higher than 100 ms, bandwidth increase beyond 3 Mbps has almost no positive impact on the PLT [24]. Users can easily perceive the lags in web page load when access time suddenly increases by 100–200 ms. When the access time is above 300 ms, the page loads sluggishly, and when it goes beyond 1 s, users move on (Grigorik et al. [25]). Similar to PLT, user perceived application latency is an important QoE metric for social media based mobile applications like Facebook. The degradation in user perceived latencies can lead to frustrating experiences for its users. Chen et al. [26] find that access time is on the critical path for some user actions like photo sharing, and can contribute up to 65% of the user-perceived latency. Another important measure of QoE is the user application retention. A large-scale study by [27] on quantifying impacts of access times on application retention rate found that the application retention rate can be sensitive to increase to access times across all categories of mobile applications. They found that user retention rate (on a scale of 0–100) dropped from 98.3 to 66.5 when median access time increased from 34 ms to 79 ms for messenger based applications like Whatsapp and from 92.7 to 67.8 for a median access time increase from 37 ms to 70 ms for Twitter. Also, there have been significant efforts on the application level protocols to reduce access time latency and improve the QoE. The newly proposed HTTP/3 [28] standard uses the QUIC transport protocol for the web. QUIC runs in the application layer on top of UDP, instead of TCP, therefore no additional handshakes and slow starts are required, thus reducing the connection overhead. QUIC also introduces the concept of streams that are delivered independently such that in most cases packet loss affecting one stream does not affect others. The literature studies [29]–[31] show that the PLTs using QUIC are roughly 25%–30% faster than HTTP/2 and 35%–40% faster than HTTP/1.1 in environments that have high access time latencies.

Besides the cloud access time distributions, the model should also be able to capture their time-based variations. A study by Nikraves et al. [32] shows that significant non-uniform variations in access times are possible across Mobile Network Operators (MNOs), geographic locations and different times of day, thus making the access times difficult to model and predict. Certain mobile applications like Voice over IP (VoIP), and online gaming are very sensitive to the large variation in cloud access times (jitter). A study of Skype users by Chen et al. [33] showed that the duration of VoIP sessions is directly impacted by access time and its jitter. The median duration of sessions with access times greater than 270 ms were 4 min, while sessions with access times between 80 ms and 270 ms were 5.2 min. However, when access times dropped below 80 ms the session durations doubled to 11 min. In their empirical model of user dissatisfaction, the access

time jitter parameter has a weight factor of 53%. A study by Cisco [34] recommends 30 ms as the acceptable jitter threshold for VoIP applications.

For online gaming applications, Wang et al. [35] define Game Mean Opinion Score (GMOS) metric for measuring their QoE. The GMOS metric has a range from 1.0 to 5.0, where 4.5–5.0 means an excellent game with no impairments, 3.0–4.0 implies a noticeable impairment, where the user might quit the game, and 1.0–2.0 means an annoying environment where the user will definitely quit the game. They found that the GMOS in general decreases with an increase in access time. Their measurement-based study of gaming experience on-campus WiFi network concludes that although generally, GMOS greater than 4.0 is achievable on WiFi, there are also frequent periods of network instability when access time suddenly can increase by 200 ms which leads to a drop in user experience (GMOS-2.0). Pantel et al. [36] show that backend access time latencies over 100 ms can create paradoxical situations in real-time multiplayer racing games. Studies in [37] for First Person Shooting (FPS) games found that for backend access times above 100 ms, the hit rate of precision shooting reduced by more than 50%, thus putting certain players at disadvantage. In contrast, Real Time Strategy (RTS) games are more tolerant to backend access times. Sheldon et al. [38] study the effect of backend access time on players of the RTS game Warcraft III and conclude that while the latency of several seconds are noticeable for players, it has little to no effect on the game outcome.

The above studies of various categories of mobile applications demonstrate the dependence and the sensitivity of QoE on the access time distribution and their time-based variations and the need to model them accurately.

III. CLOUD ACCESS TIME MODELING

In this section, we discuss the background of our work by presenting the Long Short Term Memory (LSTM) neural net framework which we have chosen for modeling cloud access times. Next, we introduce the transfer learning process used to build target environment specific cloud access time models from pre-trained LSTM neural net models.

A. The Long Short Term Memory (LSTM) Neural Net Framework

Let a random variable x_t represent the time required to access a real cloud service in a given domain \mathcal{D} at time t . The domain here implies a combination of the end-user context, a real mobile device, a real access network, and a real cloud backend service. Given some constant measurement frequency, the real cloud service access time traces for the domain \mathcal{D} can be represented as a discrete-time series vector $X_D = [x_{D1}, x_{D2}, \dots, x_{DZ}]$ of length Z measured over a certain time period. A basic synthetic trace generation problem can then be expressed as modeling a prediction function F that uses X_D to generate the cloud access time $\hat{x}_{D(Z+1)}$ of the domain \mathcal{D} in the next time step $Z + 1$.

$$\hat{y} = \hat{x}_{D(Z+1)} = F(x_{D1}, x_{D2}, \dots, x_{DZ}) \quad (1)$$

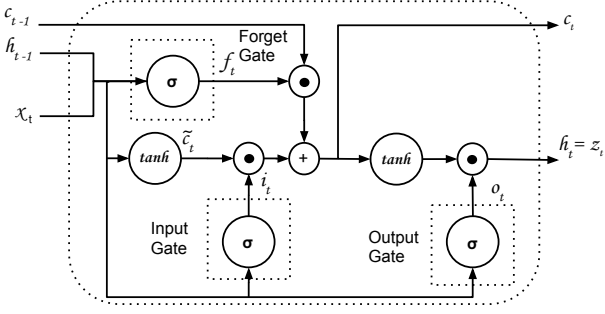


Fig. 2: Typical Long Short Term Memory (LSTM) cell unit.

The analytical framework that we apply to the trace generation problem is “Long Short Term Memory” (LSTM) neural net [39]. LSTM is a state of the art deep learning model which can capture the temporal structures within the traces at different resolutions, including both long-term as well as short-term. LSTM has been consistently used in the literature for time series prediction problems [40]–[42] and proven to be stable and powerful.

We use a typical LSTM cell unit shown in Figure 2 and described by the equations in 2–7. $\sigma(\cdot)$ is a sigmoid function that limits a real valued input between $[0, 1]$ and $\tanh(\cdot)$ represents the hyperbolic tangent function that limits the real valued input in the $[-1, 1]$ range. The \odot represents element-wise multiplication, and t is the time step. The LSTM cell consists of a hidden state $h_t \in \mathbb{R}^N$ with N hidden units, an input modulation gate $\tilde{c}_t \in \mathbb{R}^N$, and three gates, the input gate $i_t \in \mathbb{R}^N$, the forget gate $f_t \in \mathbb{R}^N$, and the output gate $o_t \in \mathbb{R}^N$. The memory cell unit $c_t \in \mathbb{R}^N$ accumulates the state information at time step t and is the sum of the previous memory cell unit c_{t-1} modulated by f_t and the input gate i_t modulated by \tilde{c}_t which is a function of the current input x_t and previous hidden state h_{t-1} . Gates are a mechanism to optionally pass the input through them in order to update the cell state. Whenever a new input arrives, its information is accumulated in the cell if the input gate i_t is activated. The prior cell status c_{t-1} at step $t-1$ is forgotten if the forget gate f_t is activated. Similarly, the output gate o_t learns how much of the memory cell to transfer to the hidden state h_t . W_{xj} , W_{hj} , and b_j where ($j = i, f, o, c$) are the parameters of the cell unit that are learned during the training.

$$i_t = \sigma(W_{xi}x_t + W_{hi}h_{t-1} + b_i) \quad (2)$$

$$f_t = \sigma(W_{xf}x_t + W_{hf}h_{t-1} + b_f) \quad (3)$$

$$o_t = \sigma(W_{xo}x_t + W_{ho}h_{t-1} + b_o) \quad (4)$$

$$\tilde{c}_t = \tanh(W_{xc}x_t + W_{hc}h_{t-1} + b_c) \quad (5)$$

$$c_t = f_t \odot c_{t-1} + i_t \odot \tilde{c}_t \quad (6)$$

$$h_t = o_t \odot \tanh(c_t) \quad (7)$$

The network can make use of multiple LSTM units stacked on top of each other to make the network deeper. The stacking of memory units on top of each other causes the hidden

states to be propagated to the deeper layers, thus enabling the hierarchical processing of time series data. An end-to-end network path can exhibit temporal dynamics at different time scales within the trace time series. Thus, stacking the layers on top of each other may enable the processing of this temporal hierarchy.

B. Transfer Learning

A domain \mathcal{D} consists of an input feature space \mathcal{X}_D and a marginal probability distribution $P(X_D)$, where $X_D = [x_{D1}, x_{D2}, \dots, x_{DZ}]$ and $X_D \in \mathcal{X}_D$. Thus, given a domain $\mathcal{D} = \{\mathcal{X}_D, P(X_D)\}$, and the output feature space \mathcal{Y}_D , the goal of a task $\mathcal{T}_D = \{\mathcal{Y}_D, F_D(\cdot)\}$ is to learn a prediction function F_D using the training data pairs $D = [(x_{D1}, y_{D1}), (x_{D2}, y_{D2}), \dots, (x_{DZ}, y_{DZ})]$, where $x_{Di} \in \mathcal{X}_D$ and $y_{Di} \in \mathcal{Y}_D$. In the case of time series prediction problems, both the input and the output space are the same i.e $\mathcal{X}_D = \mathcal{Y}_D$. Therefore, $x_{Di}, y_{Di} \in \mathcal{X}_D$. Further, since the prediction is carried out single step at a time, y is obtained by shifting x by one, i.e. $y_i = x_{i+1}$. Thus, given an input access time x at the current time step, the prediction function F_D is used to predict the output access time at the next time step. F_D can also be expressed as a conditional probability distribution function $P(y|x)$.

Figure 3 shows the comparison of the transfer learning approach with the traditional machine learning approach for the access time prediction problem. We consider two domains: the source domain \mathcal{D}_S (an indoor environment such as a cafe with a stationary mobile device accessing a cloud backend service on a LTE network) and the target domain \mathcal{D}_T (an other indoor environment like an office with a different stationary mobile device accessing an other cloud backend over an other LTE network). In the source domain $\mathcal{D}_S = \{\mathcal{X}_S, P(X_S)\}$, using the measured access times data pairs $D_S = [(x_{S1}, y_{S1}), (x_{S2}, y_{S2}), \dots, (x_{SZ}, y_{SZ})]$ a source task \mathcal{T}_S has learned a prediction function F_S . We call this a pre-trained model (Model S in Figure 3). Now in the target domain, $\mathcal{D}_T = \{\mathcal{X}_T, P(X_T)\}$ a short sample of the access time is measured. This access time sample is represented by the vector $X_T = [x_{T1}, x_{T2}, \dots, x_{TM}]$ of length M such that $0 < M \ll Z$. Given the training data pairs $D_T = [(x_{T1}, y_{T1}), \dots, (x_{TM}, y_{TM})]$ such that $x_{Ti}, y_{Ti} \in \mathcal{X}_T$, transfer learning for access time prediction in \mathcal{D}_T is defined by a target task $\mathcal{T}_T = \{\mathcal{Y}_T, F_T(\cdot)\}$. In transfer learning, \mathcal{T}_T learns a prediction function F_T (Model T in Figure 3) using both the training data pairs D_T and also the knowledge in D_S and \mathcal{T}_S (pre-trained Model S). Further, we consider $D_S \neq D_T$, since the marginal probability distributions of the source and the target domains are different i.e $P(X_S) \neq P(X_T)$.

IV. SYNTHETIC ACCESS TIME TRACE GENERATION

In this section, we present the methodology for using transfer learning to address the problem of modeling cloud access times for target environments. First, we explain the details of context-driven network testing scenarios and cloud access time data collection, and our archive of cloud access time traces.

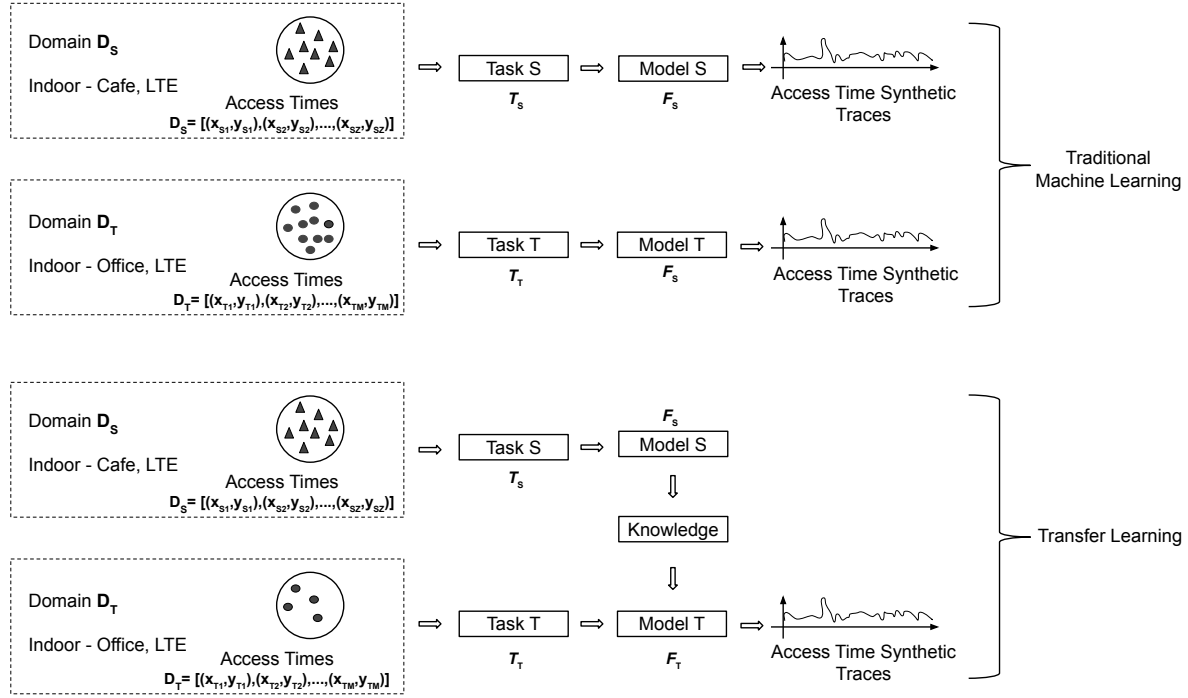


Fig. 3: Traditional machine learning vs. Transfer learning approach to access time prediction.

Next, we explain our approach to building the source model library. The pre-trained model library forms the basis for our transfer learning to enable rapid model building and trace generation of target environments. Based on the earlier transfer learning studies in other domains [43], we hypothesize that transfer learning performance is highly impacted by the choice of the pre-trained source model used for learning, the number of layers to be transferred in the learning, and the amount of target environment data available for learning. Therefore, we carefully design experiments to characterize transfer-learning performance of cloud access time models under the impact of these factors.

A. Cloud Access Time Trace Collection

Since there are no readily available pre-trained LSTM models for mobile cloud access times, we build them ourselves. We use the LSTM neural net architecture framework consisting of a stack of LSTM cell units as our pre-trained source models. Furthermore, there are no publicly available datasets for mobile cloud access time series. The access times and the network performance has been known to exhibit a high degree of correlation to the end-users location, environment, and the situation [8]; the factor we refer to as context in this paper. Thus, these access time measurements need to be labeled with appropriate context information that could then be used to build LSTM models. Inspired by the previous work Imagenet [44] in the machine learning domain, we build an archive of cloud access time traces for a selected set of contexts.

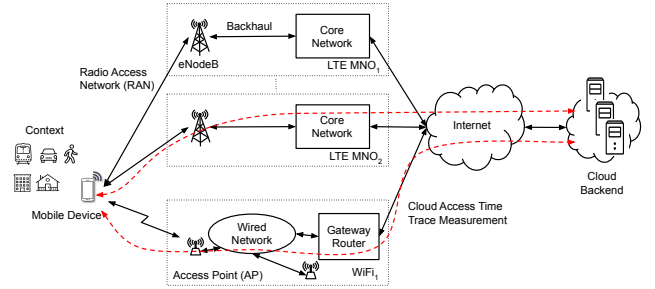


Fig. 4: Experimental setup for collecting cloud access time traces on the LTE and WiFi networks for different contexts. The end-to-end network path for cloud access time measurement is shown with the red dashed line.

1) *Measurement Setup and Scenario:* Our experimental setup for collecting cloud access time measurements is shown in Figure 4. We collect cloud access time measurements for a combination of a mobile device, cloud backends, and access networks for various end-user contexts. The different contexts include the mobile scenarios of users in the outdoor urban environment with walking, vehicle, and train commutes. We also considered stationary end-user scenarios at various urban locations in indoor environments such as home, office, dormitory, and cafe. It is common for mobile applications to use backend servers hosted in the public cloud. Therefore, we use AWS to host the backend, as it is well provisioned with high availability across different geographical regions and it is easier to isolate and model the impact of access

TABLE I: Overview of the cloud access time dataset archive showing different contexts, locations (DE - Germany, US - United States), network types (LTE, WiFi) and mobile network operator (MNO) on which measurements were carried and their respective RTT counts.

Context		Cloud access time dataset			
Type	Scenario	LTE		WiFi	
		Location	Count	Location	Count
Mobile	Train	DE (MNO_1)	30K	-	-
	Vehicle	DE (MNO_1)	30K	-	-
	Walking	US (MNO_2)	30K	DE (Campus)	30K
		DE (MNO_3)	30K		
Stationary	Indoor	DE (MNO_1)	30K	DE (Home)	30K
				DE (Office)	30K
				DE (Dorm)	30K
				US (Cafe)	30K
	Outdoor	DE (MNO_3)	30K	DE (Cafe)	30K

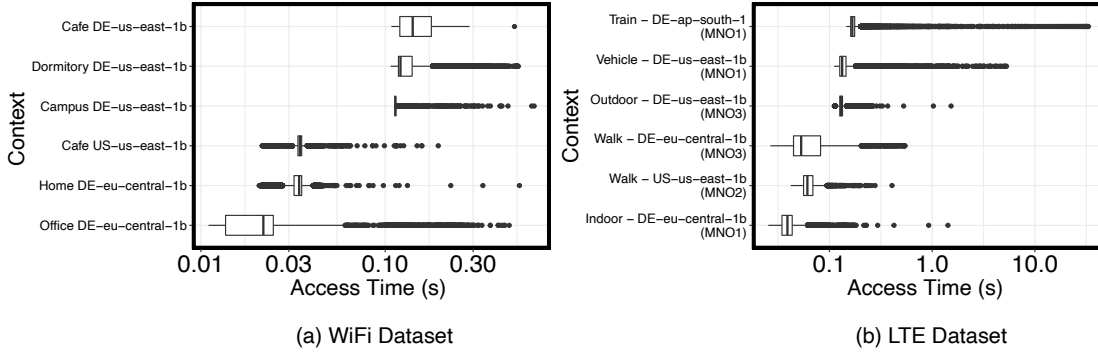


Fig. 5: Boxplots of our WiFi and the LTE datasets consisting of 30 000 cloud access time (RTT) samples for different contexts. The box in the figure is defined by the 25th, 50th, 75th percentiles. And the access times are plotted on base 10 logarithmic scale.

times. The application backend server is hosted on a Virtual Machine (VM) in three different geographical regions of AWS data-center — United States (Virginia), Europe (Frankfurt), and Asia Pacific (Mumbai). The access network connects the mobile device to the cloud backend. For our measurements, we consider WiFi networks and LTE cellular networks from different Mobile Network Operators (MNOs).

The scope of our data collection is in no way extensive. The context environments were selected based on common mobile application network testing scenarios. On the other end, the access networks are limited to LTE and WiFi. These data collection could be extended as needed for a given class of access networks, end-user locations and contexts, and the cloud backends geographically distributed over various regions. In fact, we plan to expand their scope to include 5G as a part of our future work.

For each cloud access time measurement, we fix the context, connect the device to a selected network, and select an application backend. In the case of WiFi, we have collected measurements in total on six different networks including public and private WiFi networks. In order to collect measurements on cellular networks, we have used LTE from three different Mobile Network Operators (MNOs) in two countries — United States (US) and Germany (DE).

2) *Cloud Access Time Measurement*: We define the cloud access times as the network Round Trip Time (RTT) between

the mobile device and the cloud backend. The network RTTs are measured for each context mentioned in Table I. The RTTs are measured using our prototyped *ContextPing* Android application. *ContextPing* uses the ported standard native UNIX ping utility tool based on ICMP. It enables the configuration of the cloud application backend to which the access time should be measured, the frequency with which ICMP packets are sent, and the total time duration of the measurement. Each of our RTT time series measurement dataset lasts for a time duration of 15 000 s (4 h and 10 min) and consists of 30 000 ICMP packets generated with a time interval of 500 ms. All our cloud access time datasets were collected using a Samsung A70 mobile phone that ran *ContextPing* on the Android 9.0 Operating System. An overview of our trace collection is shown in Table I. The boxplots for the WiFi and the LTE cloud access time datasets are shown in Figure 5a and b, respectively. In the remainder of the paper, we refer to each of these 30 000 RTT measurement samples as a single dataset.

B. Building Source Model Library

1) *Performance Metric*: There are several performance metrics such as Root Mean Squared Error (RMSE), Mean Absolute Error (MAE), Mean Absolute Percentage Error (MAPE), Symmetric Mean Absolute Percentage Error (SMAPE), etc. that are used for evaluating the accuracy of

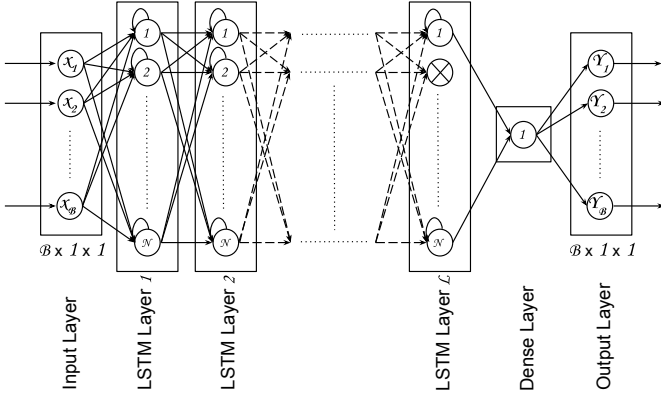


Fig. 6: Our LSTM based source model architecture.

trace models that generate time series data (see [45]). Both RMSE and MAE are unit dependent measures. MAPE is the most widespread metric for evaluating time series prediction accuracy. However, it places a heavier penalty on predicted values that exceed the real value [46]. Further, it biases the estimate if the real values are small or zero. Symmetric Mean Absolute Percentage Error (SMAPE) introduced by Makridakis et al. [47] is more balanced in handling smaller real values. Although the name suggests otherwise, SMAPE is asymmetric by nature while MAPE is symmetric (see [48]). SMAPE has been widely used in time series prediction problems like demand prediction during extreme events at Uber [49], predicting electricity load during peaks [50] etc. Therefore, we use a scaled version of the SMAPE performance metric proposed in [45] for our pre-trained source model evaluation. It is defined as follows:

$$SMAPE = \frac{100\%}{N} \sum_{i=1}^N \frac{|y'_i - y_i|}{|y_i| + |y'_i|} \quad (8)$$

where y'_i is the model predicted value of the i_{th} data-point in the time series and y_i is the real value.

2) **Building Source Models: Source Model Architecture** — Our goal is to find a specific instance of the source model architecture for each of the selected contexts. We use the general architecture shown in Figure 6. The input layer is connected to L stacked layers of LSTM cell units followed by the dense layer and the output layer. The number of stacked layers of LSTM cell units (L) can vary for each source dataset. N is the number of hidden units in each of the LSTM units. Overfitting can be a serious problem in training LSTM based architectures, therefore a dropout function is commonly used to avoid overfitting. A dropout function randomly drops hidden units during the training, and thus allows different units to learn and prevents co-adaptation among them. It is known to improve neural net performance [51]. Therefore, in the final LSTM layer L , a dropout function is applied. A dense layer is an activation function that maps the multi-dimensional input received after the dropout in the last LSTM layer to the output which is the predicted value of access time. An activation function should be able to output values that are far from

the mean and median values with higher probabilities, and thus preserve the long tail nature of access time RTTs. An activation function like Exponential Linear Unit (ELU) [52] satisfies this requirement. The ELU function is defined as x if $x > 0$ and $\alpha \cdot (\exp(x) - 1)$ if $x < 0$. Thus, ELU is an identity function for positive inputs. And for the negative inputs, the output is smoothed towards the hyperparameter α . Thus, α controls the value to which an ELU saturates for negative inputs. However, ELU is deterministic by nature and exhibits a fixed input-output relationship, thus limiting its generalization ability. In order to obtain better generalization, we add a stochastic perturbation $\sigma\epsilon$ to ELU, where σ is the range of stochastic perturbation and ϵ is randomly sampled from $\mathcal{N}(0,1)$. This stochastic activation function was proposed by Lee et al. [53] and is called Probabilistic Activation (ProbAct). In our ProbAct activation function, an ELU function is used with $\alpha = 1.0$, $\sigma = 1.0$. The input layer takes as input a single data-point x_i of the cloud access time series and the output layer outputs the predicted value y_i which is the next time step in the time series. For training, the input layer is a tensor of dimension B , where B is the batch size parameter that would be used in training this architecture and is explained later.

Training and Testing Data Splits — We split each of the cloud time series datasets, i.e., $[x_1, \dots, x_Z]$ into two subsets preserving the ordering of the time series. The training set, $S_{Training}$, consists of x_1, \dots, x_P (where $P < Z$) and is used for training the architecture. The testing set, $S_{Testing}$, consists of $[x_{P+1}, \dots, x_Z]$ and is used for testing. This split is made in an 80:20 ratio such that 80% samples (24000 RTT pings) in the time series are in $S_{Training}$ set and the remaining 20% (6000 RTT pings) in the $S_{Testing}$ set.

Preprocessing — Data cleaning and processing is a precursor step to training a model. In this step, we standardize the $S_{Training}$ and $S_{Testing}$ datasets separately. Standardization is defined as subtracting the mean value and dividing by the standard deviation of the dataset from each data point in the dataset. Standardization makes the dataset scale-invariant, thus enabling the model to generate cloud access time traces across multiple data scales.

Next, we transform the $S_{Training}$ and $S_{Testing}$ datasets into labeled datasets such that it is suitable for training LSTM architecture in a supervised manner. This means for every data-point (input feature) in the input $S_{Training}$ time series, we have an output data-point (output feature). Since our LSTM architecture predicts one step at a time, the output ground truth time series is obtained by shifting the input time series by a factor of one. Each data-point y_i in the output time series is the x_{i+1} data-point in the input time series. Thus, the $S_{Training}$ and $S_{Testing}$ datasets are transformed into tensors of $P \times 2 \times 1$ and $(Z - P) \times 2 \times 1$ dimensions, respectively.

Training — The goal of the training is to identify suitable weights that minimize a loss function using the transformed labeled $S_{Training}$ dataset. We use the Mean Squared Error (MSE) between the estimated and the actual data-points in the output time series of the labeled $S_{Training}$ dataset as the loss function for our training.

For training, we use the gradient descent based optimization algorithm based on adaptive learning rates called Adam proposed by Kingma et al. [54]. The Adam optimizer is described in Algorithm 1 and can be explained as follows. $f(\theta)$ is the stochastic objective function whose expected value $E[f(\theta)]$ is to be minimized with respect to parameters θ . $f_1(\theta) \dots f_T(\theta)$ denote the value of the function over each time-step $1, 2, \dots, T$. And $g_t = \nabla_{\theta} f_t(\theta)$ denotes the gradient, i.e. the vector of partial derivatives of f_t with respect to θ at time-step t . The algorithm evaluates the exponential moving averages of the gradient (m_t) and the squared gradient (v_t) at each time step t . The hyper-parameters $\beta_1, \beta_2 \in [0, 1)$ control the rate of exponential decay of moving averages. These moving averages are the estimated 1st moment (the mean) and the 2nd raw moment (the uncentered variance) of the gradient. Since the moving averages are initialized to zeros, their estimates are biased towards zero. This is particularly noticeable during the initial time-steps and when the decay rates are small. Therefore, a bias correction factor is applied to obtain \hat{m}_t, \hat{v}_t . The bias corrected estimates are then used to take a time-step Δ_t in parameter space which is equal to $\alpha \cdot \hat{m}_t / (\sqrt{\hat{v}_t} + \epsilon)$. As the learning rate α is responsible for selecting the magnitude of these parameter space steps, it can be adapted in such a way so that the optima is reached in few iterations.

Algorithm 1: Adam Optimization as proposed in [54].
Symbol g_t^2 indicates the elementwise square $g_t \odot g_t$.
Learning rate is denoted as α and set to 0.00001.
Hyper-Parameters are set to $\beta_1 = 0.9$, $\beta_2 = 0.999$,
and $\epsilon = 10^{-7}$

Input: $f(\theta)$ with parameters θ
1 Init: $\theta_0, m_0 = 0, v_0 = 0, t = 0$
2 while θ_t not converged **do**
3 $t \leftarrow t + 1$
4 $g_t = \nabla_{\theta} f_t(\theta_{t-1})$
5 $m_t \leftarrow \beta_1 m_{t-1} + (1 - \beta_1) g_t$
6 $v_t \leftarrow \beta_2 v_{t-1} + (1 - \beta_2) g_t^2$
7 $\hat{m}_t \leftarrow m_t / (1 - \beta_1^t)$
8 $\hat{v}_t \leftarrow v_t / (1 - \beta_2^t)$
9 $\theta_t \leftarrow \theta_{t-1} - \alpha \cdot \hat{m}_t / (\sqrt{\hat{v}_t} + \epsilon)$
10 end
11 return θ_t

Further, we train in batches of size B since the entire $S_{Training}$ data may not fit in the memory in a single run. We use different batch sizes (B) in training from 4 to 32 in increments of power of 2. The batched data is fed without shuffling to the LSTM architecture, thus preserving the order of data-points. We also ensure that each LSTM cell retains its state while training across the batches as we have a single time series input that spans multiple batches. In order to get the optimizer to converge, we train the architecture over multiple cycles through the entire training dataset. Each such cycle is referred to as the epoch. We vary the number of epochs from

100 to 700 in increments of 100.

TABLE II: Hyperparameters of the architecture and training

Type	Hyperparameter	Space
Architecture	Number of stacked layers of LSTM cell units (L)	1, 2, 3, 4
	Hidden units (N)	8, 16, 32, 64, 128, 256, 512
	Dropout	0.5
	Dense layer activation function	ProbAct [53] with ELU $\alpha=1.0$ perturbation $\sigma=1.0 \epsilon=\mathcal{N}(0,1)$
Training	Batch Size (B)	4, 8, 16, 32
	Epochs	100 - 700
	Learning Rate	$\alpha=0.00001$

Hyperparameters Tuning & Testing — The hyperparameters (highlighted in Table II) of the architecture include the number of layers of stacked LSTM cell units (L). We vary the number of stacked layers of the LSTM units in the architecture from 1 to 4. The number of hidden units (N) in each LSTM cell unit of the stacked layers are varied from 8, 16, 32, 64, 128, 256, 512. The dropout function value is set to 0.5 which has been shown by Srivastava et al. [51] as being close to the optimal for a wide range of networks and training tasks. After carrying out the hyperparameter tuning, we select the parameterization with the minimum MSE loss on the $S_{Testing}$ set as the pre-trained source model. Thus, in the end, we have a separate source model for each dataset in the archive. Each of these source models can have different numbers of stacked layers and also differ in the values of other hyperparameters.

Implementation — The source model architecture is implemented in Python using the open-source deep-learning library Keras [55] and uses the Tensorflow backend. Our source model training is executed in the AI Platform service from the Google Cloud Platform (GCP). We run our experiments on a GCP predefined scale tier cluster consisting of a *n1-standard-4* instance type and includes a single worker instance. We found this tier to be suitable for training the source models after initial experimentation. The total cumulative duration for the model training, including the hyperparameter tuning, across all source datasets, takes around three days.

C. Transfer Learning for Target Environment Model Generation

In the following, we describe the experiments designed to evaluate the robustness of transfer learning for various targeted context environments on WiFi, and LTE networks.

1) *Selection of Pre-trained Models for Fine-tuning:* Earlier studies [43] have shown that within a specific architecture, using transfer learning with fine-tuning of arbitrarily chosen source model can not only improve but also worsen the model accuracy compared to when the model is trained from scratch. This phenomenon is known as a positive and negative transfer, respectively. Therefore, we need to select the source models for fine-tuning in an informed manner. The source model selection criteria should also make it easy for application testers to quickly select the optimal source model for the target environment of interest. The authors in [56] show that

selecting a source model whose dataset characteristics are similar to the target dataset characteristics can increase the likelihood of positive transfer learning. Therefore, we use a similarity distance measure for time series called Dynamic Time Warping (DTW) proposed in [57] for selecting the source model. DTW is an elastic measure that optimally aligns the time series in the temporal domain. Thus, it also works when the two time series have different lengths and have been sampled with different frequencies.

2) *Transfer Learning Organization*: The Target Domain (D_T) experiment consists of using transfer learning to fine-tune a model from pre-trained Source Domain (D_S) with the access time sample of D_T . We split the D_T trace sample into two sets, $T_{Training}$ and $T_{Testing}$, which are respectively used for training and testing the D_T model. As earlier, we also standardize the target datasets separately. Next, we select a pre-trained D_S model and freeze the weights in the initial LSTM layers of the architecture (starting from LSTM layer one) and then fine-tune on the remaining LSTM layers. We hypothesize that when stacking the LSTM layers to build a D_T model, the weights in the initial layers are more representative of the learning of the generic features present in time series data. Thus, these features learned on the D_S can be used in the D_T . On the other hand, the final layers in the architecture are closely related to the predictive component of the model. We transfer the weights of the initial layers in D_S by freezing them and fine-tune the model using the target $T_{Training}$ set on the final layers. Thus, we transfer the learnings carried out in the D_S model into fine-tuning the D_T model. The D_T model

is tested using $T_{Testing}$. We study the impact of the following factors on the transfer learning performance.

Impact of the source and target dataset similarity — To study the impact of source and target dataset similarity on the transfer learning performance, we carry out transfer learning between each pair of the dataset in our archive. We use the source models trained in the earlier step for transfer learning. The DTW distance measure characterizes the dataset similarity.

Impact of the number of transferred layers — In transfer learning to obtain a target model, fine-tuning is carried out only on a subset of layers from the pre-trained source model while retaining the weights of the remaining subset of layers by freezing them. We also study the impact of the number of transferred layers on the transfer learning performance.

Impact of the amount of target data — To evaluate the impact of the amount of target environment data available for fine-tuning the model, we vary the size of the target dataset used in fine-tuning.

3) *Performance Metric for Transfer Learning*: For a target environment, we introduce the notion of a specialized model. A specialized model is obtained by training from scratch on the target environment data as if no pre-trained source model existed. A specialized model can be obtained by using the training process defined in Section IV-B2. The specialized models provide the baseline performance for transfer learning. As a performance metric, we consider the percentage improvement in the SMAPE of the fine-tuned model compared to a specialized model. It is computed as follows:

$$\frac{(SMAPE_{specialized-model} - SMAPE_{fine-tuned-model})}{SMAPE_{specialized-model}} \times 100 \quad (9)$$

A positive value of SMAPE improvement percentage indicates that a fine-tuned model is better than training the specialized model. On the other hand, a negative value indicates that the fine-tuned model is worse than the specialized model.

4) *Analysis Methodology*: In the following, we briefly describe how we analyze the transfer learning experiment results. To study the impact of source and target dataset similarity on transfer learning, we carry out transfer learning across all pairs of datasets in our archive by transferring the initial LSTM layers of the pre-trained source model architecture. This gives us a set of fine-tuned models. Then, for each target environment, we also train a specialized model. Finally, we also compute the DTW for each dataset pair and study if there exists a correlation between the DTW distance measure and the transfer learning performance using the SMAPE improvement metric.

For studying the impact of the number of transferred layers on the transfer learning performance, we select the pre-trained source model based on minimum DTW distance. The initial

LSTM layers in the architecture are known to represent the generic features of the access time series data that are not specific to a particular dataset and in general applicable across different datasets [58]. Therefore, for this study, we carry out transfer learning by varying the number of transferred layers from 1 to 3 beginning from the first LSTM layer to the last LSTM layer in the architecture. For each transferred layer, we carry out ten runs of out-of-sample validation typically used in time series modeling.

To study the impact of the size of target environment data used in fine-tuning on the transfer learning performance, we split the target data into different ratios consisting of 20:80, 40:60, 60:40, and 80:20 for training and testing, respectively. We then use the training subset to fine-tune the pre-trained source model. The pre-trained source model for each target environment is selected based on the minimum DTW similarity measure. In each of the fine-tuning, we set the number of transferred layers to one, and carry out ten runs of out-of-sample validation.

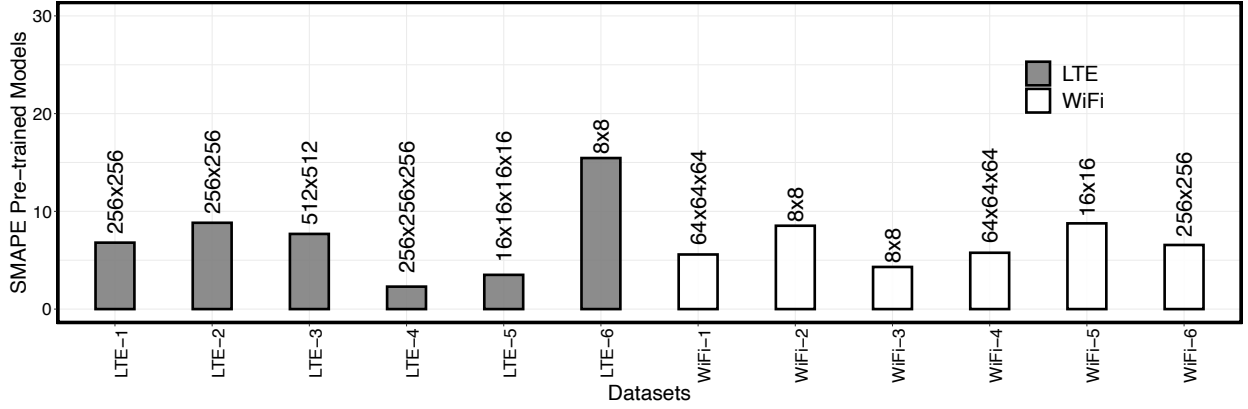


Fig. 7: Bar plots illustrating SMAPE of the source model architecture evaluated on the test data of each WiFi and LTE dataset in the archive.

V. RESULTS AND ANALYSIS

In the following, we present our results across the six WiFi and the six LTE datasets in the archive obtained using the described methodology.

A. Pre-trained Source Model

In this section, we describe the results of training the source models. Figure 7 shows the results of each of the six WiFi and LTE datasets, respectively. For each case, we report the SMAPE performance metric on the 20% testing dataset. The diversity in the SMAPE performance metric within the WiFi and the LTE datasets is visible in the figure. The SMAPE of LSTM architecture for the WiFi datasets are in the range of 5% to 8.1% while that for LTE datasets vary between 2.3% to 15.4%. All source models except the one for LTE have SMAPE below 10%, thus showing a good prediction power for the model.

The text on the top of the bar indicates the source model architecture selected for each dataset. For example, $8 \times 8 \times 8$ implies a stack of three-layered LSTM architecture with 8 hidden units in each of the layers. The dropout layer and the dense layer in the architecture are not included in the notation for the sake of simplicity. We can see in Figure 7 that the best-fit source model of every dataset has a different number of stacked LSTM layers. In the case of WiFi datasets, the number of stacked LSTM layers vary from 2 to 3, while for the LTE datasets, the number of LSTM layers vary from 2 to 4. Likewise, the number of hidden units in each of these LSTM architectures are also different. We also analyzed each of the datasets and their LSTM architectures representing them and found that datasets with longer tails have comparatively deeper LSTM architectures. In our experiments, we observed that the MSE loss function of the training stops improving after 700 epochs and that using a batch size of 16 in the training leads to minimal loss value. We use these architectures as pre-trained source models in our transfer learning experiments.

B. Transfer Learning

To understand the underlying factors impacting the performance of transfer learning, we first focus on characterizing the influence of pre-trained source model selection. Next, we study factors such as the number of transferred layers and the size of the target data used in the model fine-tuning.

1) *Pre-trained Source Model Selection for Fine-tuning*: We carry out transfer learning across each pair of the datasets in the archive (introduced in Section IV-A) by fine-tuning the source model while treating other datasets as the target data. Thus, we fine-tune 30 models for the WiFi and LTE each. In the fine-tuning, the single first layer from the pre-trained source model is transferred, while the higher layers are fine-tuned.

Figure 8a and b illustrate the heatmap of SMAPE improvement obtained from fine-tuning a source model against just training the specialized model from scratch for WiFi and LTE datasets respectively. The values along the diagonal from bottom left to top right can be ignored as they represent the same datasets. The values inside the heatmap tile depict the percentage of SMAPE improvement in the target model obtained from fine-tuning the source model. Positive values indicate that the SMAPE accuracy of the target model after fine-tuning using transfer learning is better than that of the specialized model trained from scratch, while the negative values imply that the fine-tuned target model is worse than the specialized model.

In the case of WiFi-based target models, we observe SMAPE improvements in only 46% of the cases out of 30, while for the LTE-based target models, this value drops to 33%. The positive SMAPE improvements for the WiFi models range from 0.1% to 10.7% and are marginal in the majority of the cases. In comparison, the LTE models exhibit a much wider range of SMAPE improvement from 0.1% to 34.6%. From the negative SMAPE improvement results, we can confirm that as expected using transfer learning is not always beneficial. The positive SMAPE improvement results show that selecting certain source models can provide marginal to high accuracy

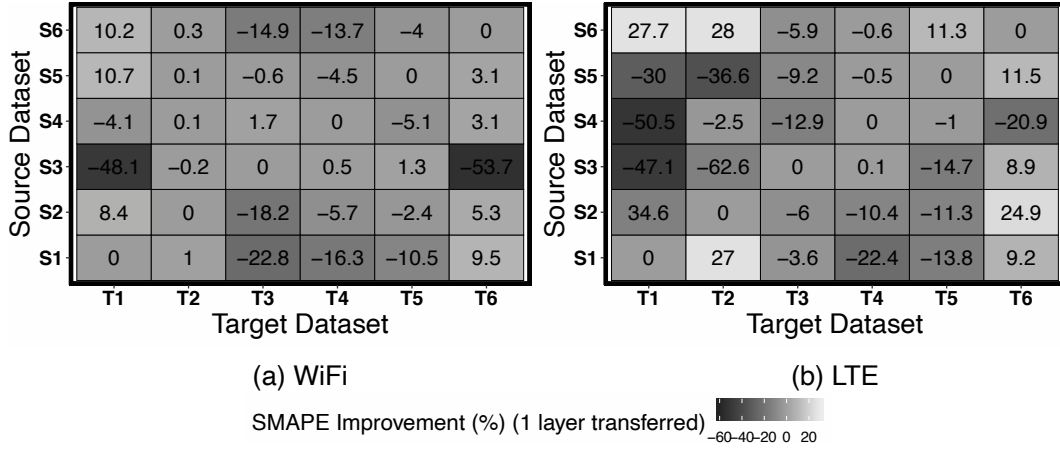


Fig. 8: Positive and negative transfer learning between the source (S) and target (T) datasets. Heatmap illustrates percentage of SMAPE improvement in the target model (obtained with fine-tuning a source model) compared to training the specialized model from scratch.

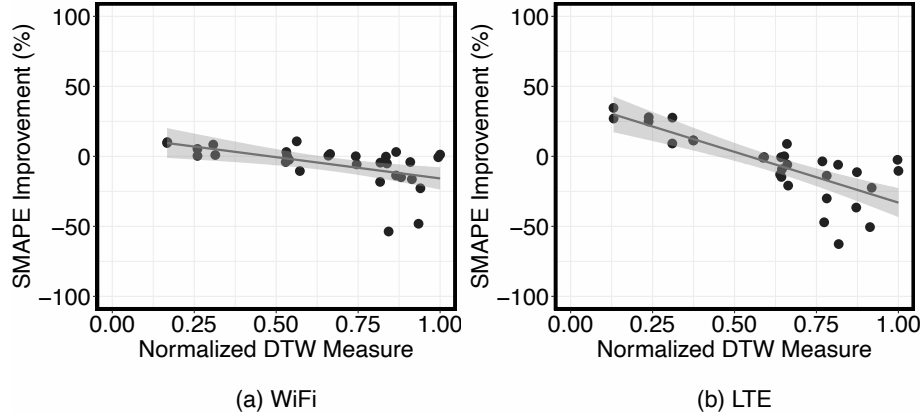


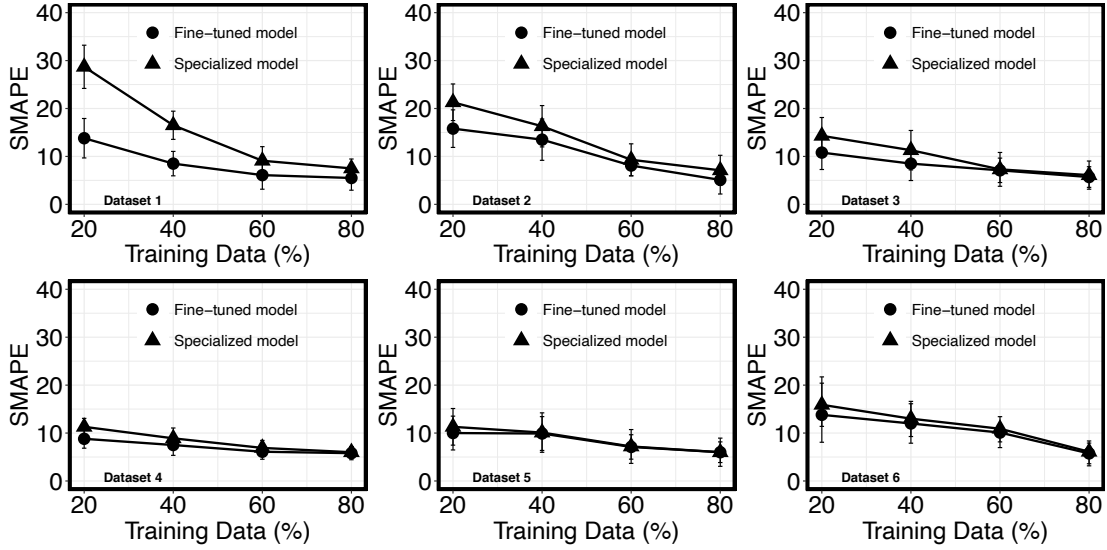
Fig. 9: Scatter plot shows SMAPE improvement in the target model against the normalized DTW measure between the source (S) and target (T) datasets. The Pearson correlation coefficient between the normalized DTW measure and the SMAPE improvement for the WiFi dataset is -0.46 and for the LTE dataset it is -0.61 , thus showing moderate to strong negative correlation.

gains. However, randomly selecting a source model based only on the network technology type, i.e., WiFi and LTE, may not offer any particular learning benefits. These results are in agreement with Wang et al. [56] and show that negative transfer results can be caused by a divergence in the joint distribution of the source and target datasets.

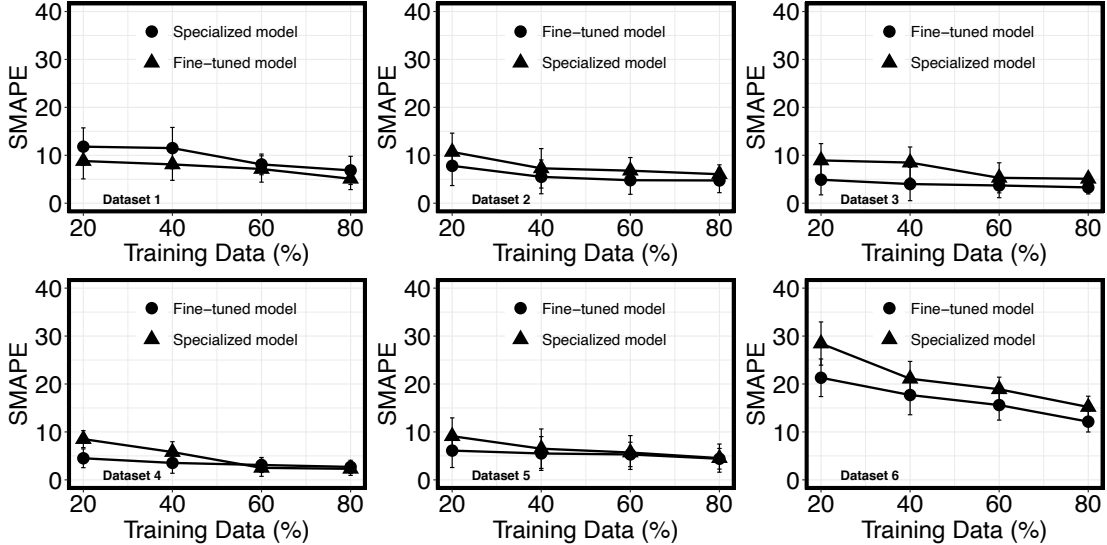
Based on the study in [57], we use the Dynamic Time Warping (DTW) distance measure for establishing similarity between the underlying source and target datasets. Figure 9a (WiFi) and b (LTE) show the scatter plots of the SMAPE performance improvement for the transfer learning between each pair of the dataset and the normalized DTW distance measure between their underlying source and target datasets. The scatter plots show that SMAPE improvement percentage indeed decreases with a decrease in the similarity between the source and target datasets. The Pearson correlation coefficient between the normalized DTW and the SMAPE improvement is -0.46 and -0.61 for the WiFi and the LTE, respectively. The

percentage of positive transfer cases jump from 46% to 83% for the WiFi and 33% to 66% for the LTE when the minimum DTW measure is used to select the pre-trained source model. From the above results, we conclude that a similarity measure like DTW is quite reliable, and using it can significantly improve the likelihood of positive transfer.

2) *Transfer Learning Scope*: In this study, we select the pre-trained source model using the minimum DTW measure between the source dataset and the target dataset. In each fine-tuning, we transfer a certain number of layers beginning from the first layer and then fine-tune only on the remaining higher layers. We vary the number of transferred layer parameter based on the number of layers defined in the source model. For example, across all our source models of WiFi and LTE datasets, only one source model consists of four LSTM layers (LTE dataset 5). In this case, we perform fine-tuning by varying the number of transferred layer parameter from 1 to 3. Likewise, in the case of source models having three LSTM



(a) WiFi Dataset



(b) LTE Dataset

Fig. 10: A comparison of the average SMAPE of the target model obtained by fine-tuning a source model and a specialized model trained from scratch for different target data sizes. The SMAPE is measured on the test dataset across 10 out-of-sample validation runs. The error bars show a 95% confidence interval. The source model for transfer learning is selected based on the minimum DTW measure between the source and the target dataset. And a single first LSTM layer was transferred.

layers, we vary the parameter from 1 to 2, and in the case of two-layered LSTM architectures, we set it to 1. We repeat each fine-tuning across 10 out-of-sample validation runs of the target dataset.

Table III shows the average SMAPE values based on the number of transferred layers for each WiFi and LTE dataset in the archive. In the case of a source model with three layers, the average SMAPE of the fine-tuned model increases as more than one layer is transferred. For a source model with four layers ($16 \times 16 \times 16 \times 16$), the SMAPE of fine-tuned model reduces until the transfer of two layers but increases thereafter.

Thus, increasing the transferred layers does not provide gains. This can be well explained by the phenomenon confirmed in the transfer learning studies in other domains [58]. The first layer in the LSTM architectures learns the generic features of the training dataset that are also applicable across other datasets while the higher layers learn features that are more training task dataset-specific. Thus, when the higher layers are transferred in the fine-tuning, it inhibits the architecture from learning the new target task dataset-specific features, thus negatively impacting the predictive power of the target model.

TABLE III: Impact of the number of transferred layers used in fine-tuning a pre-trained source model on the target model performance. The Not Applicable (NA) indicates that the specific architecture is shallower than the number of transferred layers.

Type	Target Dataset	Pre-trained Source Model	Average SMAPE by number of transferred layers		
			1	2	3
WiFi	1	8×8	5.5	NA	NA
	2	256×256	5.1	NA	NA
	3	$64 \times 64 \times 64$	5.7	10.0	NA
	4	8×8	5.8	NA	NA
	5	256×256	6.1	NA	NA
	6	$64 \times 64 \times 64$	5.7	8.1	NA
LTE	1	256×256	6.8	NA	NA
	2	256×256	4.7	NA	NA
	3	$256 \times 256 \times 256$	3.3	4.1	NA
	4	$16 \times 16 \times 16 \times 16$	2.7	2.5	4.7
	5	8×8	4.4	NA	NA
	6	256×256	12.1	NA	NA

3) *Target Training Data Size*: Knowing how much target environment data to collect to be able to generate realistic synthetic traces is critical. To answer this question, we vary the target environment data size used for fine-tuning the source model using transfer learning. In this analysis, for each target dataset, we select a source model using the minimum DTW measure. Based on our previous analysis of the impact of the number of transferred layers on the target model performance, we transfer a single layer which is the first LSTM layer of the source model and fine-tune it with the varying target data sizes.

Figure 10aa (WiFi) and Figure 10bb (LTE) illustrate the comparison of average SMAPE between a target model obtained by fine-tuning a source model, and for specialized models trained from scratch at different target data sizes. The error bars in the figures represent the 95% confidence interval across 10 out-of-sample validation runs. 20% target data size consists of 6000 RTT samples, while on the other end 80% consists of 24 000 RTT samples.

The SMAPE values of both the models across all datasets and training data sizes range from 28.7% to 5.1% for WiFi and 28.4% to 2.7% for LTE. In Figure 10aa and Figure 10bb, one can see that the SMAPE of both models increase as the data size decreases. This behavior is persistent across both the WiFi and the LTE. Also, fine-tuning has the highest performance improvement when the target data size is the smallest (20%) for both the WiFi and the LTE. The SMAPE improvements for fine-tuning case ranges from 51.9% to 3.9% in WiFi, and 47% to 25% in LTE for 20% data size. As the data size begins to increase, these gains diminish. For the largest data size of 80%, the gains are marginal (from 26% to 0% for WiFi and 35% to 2% for LTE); in the few datasets, there is no gain at all. The results very well intuitively show that obtaining a good specialized model requires a proper size of target environment data samples while fine-tuning is well done with short samples.

Another interesting aspect of the results is that for some datasets, the improvements in SMAPE between fine-tuned (for

20% data size) and specialized (for 40% data size) models are also marginal. It shows that training a specialized model from scratch using more data may not always bring in proportional performance improvements. Further, it also highlights that by selecting a transfer learning approach, one can obtain a speed up by reducing down the target environment data collection time.

The results could be used as a general guideline to estimate the minimum size of the target environment data needed to build target models of a similar context with a certain accuracy. For example, an application tester interested in building a cloud access time model for a vehicular LTE network connectivity in an urban environment can refer to our LTE Dataset 1 and Dataset 2 in the results. From the results, one can infer with a certain degree of confidence that a target environment data size of 6000 RTT samples, when fine-tuned with one of the source models, can generate a target model whose average SMAPE can vary in the range of 4.7% to 12.5%.

Further, we quantify the speed improvement resulting from the usage of transfer learning as compared to training a specialized model. We compute the speed-up factor of transfer learning as the ratio of time required to train a specialized model from scratch and the time required to fine-tune the source model. The speed-up factor is measured across 700 epochs. A single first layer of the source model is transferred for fine-tuning. The training jobs run on *n1-standard-4* virtual machine (VM) type on GCP with 4 virtual CPUs and 15 GB of memory. The vCPU is implemented as a single hardware hyper-thread on the Intel Xeon Scalable Processor (Skylake)¹ [59].

Table IV shows the comparison of the speedup factor of fine-tuning and the corresponding average SMAPE improvement percentage for all positive transfer cases across different target data sizes. The speed-up factor for a single transferred layer is similar across different data sizes and ranges from 1.1 to 1.8 for the WiFi and LTE, while the SMAPE improvement percentage varies from 1.3% to 51.9%. These results show that transfer learning not only reduces the data collection time but also speeds up the model building time without adversely impacting the target model accuracy. We conclude that carrying out transfer learning in an informed manner based on the dataset similarity rarely hurts.

VI. USAGE OF TRANSFER LEARNING IN AN EMULATION

In this section, our primary goal is to automate the process of selecting an appropriate source model, fine-tuning the source model on the target dataset, and generating synthetic access times traces using this transfer learned model. Further, we aim to integrate the synthetically generated traces within a network trace-based emulator so that it can be used in real mobile application testing. In the following, we describe our implementation efforts in this direction in the form of a tool called *ContextPerf*. In the following, we present the

¹Intel Xeon Scalable Processor (Skylake) has a 2 GHz base frequency, 2.7 GHz All-core turbo frequency, and 3.5 GHz Single-core max turbo frequency.

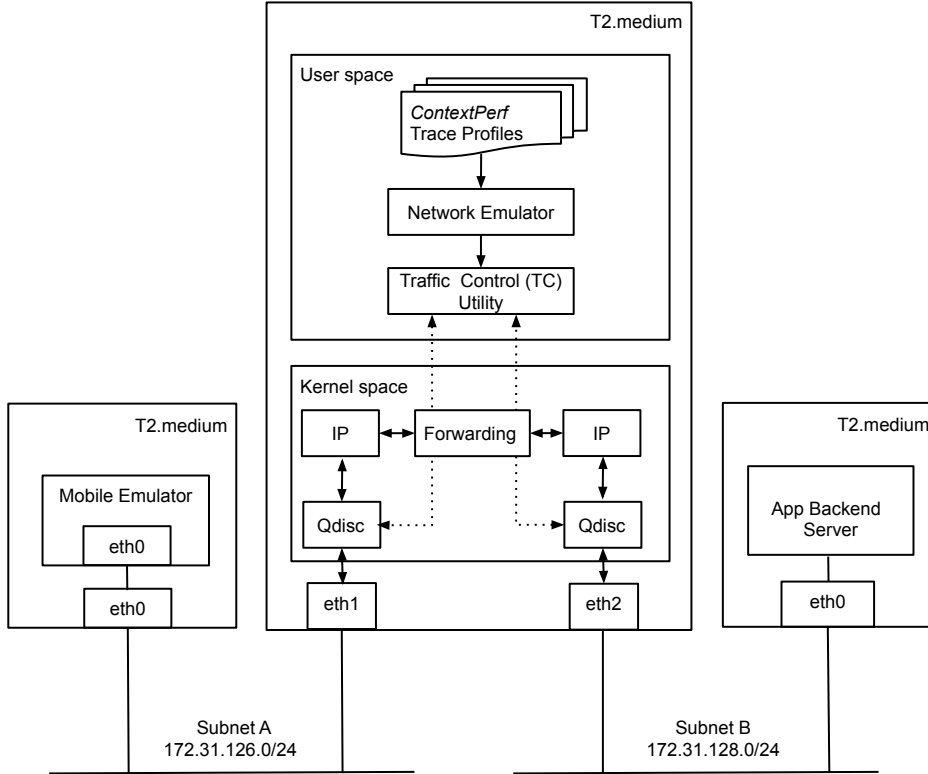


Fig. 11: Experimental setup for mobile application testing: A mobile emulator, network emulator, and application backend server hosted on separate VMs within the cloud.

TABLE IV: Fine-tuning speedup on a *n1-standard-4* virtual machine (VM) type on GCP.

	Target Dataset	Fine-Tuning Speedup				SMAPE Improvement (%)			
		20	40	60	80	20	40	60	80
WiFi	1	1.2	1.2	1.1	1.2	51.9	48.4	32.9	26.6
	2	1.2	1.2	1.5	1.2	25.8	17.1	12.9	15.1
	3	1.3	1.3	1.3	1.3	24.4	24.7	2.7	5.5
	4	1.1	1.1	1.1	1.3	22.1	15.7	11.5	3.3
	5	1.1	1.3	1.3	1.4	11.5	1.9	1.3	1.6
	6	1.3	1.3	1.2	1.3	13.2	7.6	7.3	5.7
LTE	1	1.2	1.5	1.8	1.4	34.0	25.4	29.5	11.8
	2	1.1	1.4	1.6	1.2	27.1	24.4	29.3	21.4
	3	1.1	1.1	1.3	1.2	52.8	45.1	30.1	39.2
	4	1.8	1.6	1.6	1.5	47.0	39.1	19.3	14.8
	5	1.3	1.2	1.2	1.1	33.0	15.3	7.0	2.8
	6	1.4	1.3	1.5	1.2	25.1	16.1	17.4	20.1

internals of the network emulator, and its integration with *ContextPerf* generated traces. Finally, we evaluate the end network emulation accuracy independently with real access time traces.

A. Implementation

ContextPerf is a tool written in Python that provides end-to-end automation for the generation of synthetic cloud access times traces. It takes as input a measurement sample trace file of a target environment. It standardizes the measurement

sample and selects a pre-trained source model from a model archive hosted in the cloud storage bucket. The pre-trained source model is selected based on the minimum DTW distance to the target dataset. Next, based on the input fine-tuning hyperparameters, it creates a transfer learning job in the AI platform service of GCP. Upon the fine-tuning job completion, the model and the synthetic traces generated from it are made available as files in the bucket. The synthetic trace files can then be used with any network emulator for emulating cloud access times.

We integrate these synthetic traces with the mobile network emulator developed by Akamai [17], [60]. The experimental setup for mobile application testing is shown in Figure 11. It includes the following three components: the mobile emulator that runs the application binary under test, the network emulator which emulates the cloud access times using *ContextPerf* generated synthetic traces, and the application cloud backend server. We deploy each of these components on a separate Virtual Machine (VM) in the cloud. Going forward, we limit our discussion to the network emulator component, its internal architecture, and integration with *ContextPerf* generated trace files.

As shown in Figure 11, the network emulator is hosted on a *t2.medium* VM in the AWS public cloud. The emulator requires a VM with two virtual network interfaces. One virtual

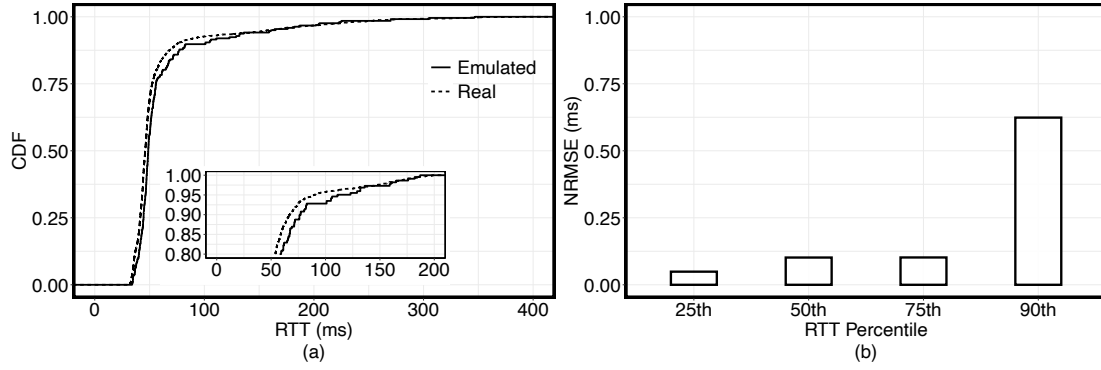


Fig. 12: (a) Cumulative Distribution Function (CDF) comparing the RTT distribution of the real RTT trace fed to the network emulator and the RTT of the emulated network path for a single emulation run of 10 min. (b) Bar-plot of the Normalized Root Mean Squared Error (NRMSE) between the real RTT and the emulated network path RTT normalized using the standard deviation of the real RTT trace for 25th, 50th, 75th, and 90th percentiles. NRMSE is calculated across 30 emulations.

network interface belongs to the subnet of the mobile emulator (the application client) and the other belongs to the subnet of the application backend server. The network emulator then uses *iptables* [61] rules with masquerading to forward traffic received on the client subnet to the server subnet and vice versa. On the client and the server VMs, the underlying routing tables are modified to route the network traffic through the network emulator VM.

The network emulator is based on the Linux Traffic Control (TC) [62]. TC is a set of utility tools that enables configuration and management of the kernel packet scheduler, and thus offers control over the packet traffic flow transmitted and received through the queueing system (*qdisc*) associated with the network interface. Using TC, one can introduce packet delays, change the rate at which packets are transmitted and received, as well as drop and re-order the packets. Thus, one can emulate the delay, bandwidth, packet loss, and re-ordering characteristics of any network path. The network emulator is available as a bash script with an in-built set of fixed network profiles.

The emulator uses time-driven emulation that updates the delay parameter of the *qdisc* after every fixed time interval. This value is set to the time interval used to generate the synthetic traces. We set it to 500 ms. The emulator internally adjusts this time interval to account for the time required to change the *qdisc* using the TC utility (4 ms).

We modified the source code of the emulator to change the delay parameter as per the synthetic traces generated by *ContextPerf*. Since *ContextPerf* generates RTT synthetic traces, we divide them to set the uplink and the downlink network path delay. We configure the network emulator to use symmetric delays for the uplink and downlink paths.

We carried out the following modifications and extensions to the core functionality of the network emulator. We added a configuration API support that enables the external feeding of the trace files as input to the emulator. It supports setting the time interval for changing the emulation parameters and customizing the ratio of the uplink to the downlink delay. We

daemonized the network emulator component by implementing it as a *systemd* service on the VM. The network emulator service is then packaged as a VM image and made available as a Terraform [63] module using the AWS provider.

B. Evaluating Baseline Emulation Accuracy

Next, we evaluate the baseline network emulator accuracy for the setup in Figure 11 in an isolated manner independent from the *ContextPerf*. Our goal is to find out how accurately the network emulator emulates the network path using the cloud access time traces fed to it. We analyze the RTT characteristics of the emulated network path between the mobile emulator client and the application backend server in Figure 11.

In the experiment, we feed a real RTT trace to the network emulator and then measure the RTT on the emulated network path. The RTT trace fed to the emulator consists of ICMP ping every 500 ms for a total of 600 pings lasting 5 min. It is measured between a real Android phone and a VM in the AWS cloud. We repeat the experiment for 30 different RTT traces measured over five Wifi and two LTE access networks.

Figure 12a shows the Cumulative Distribution Function (CDF) comparison of a real RTT trace fed as input to the network emulator and RTTs of the emulated path (Figure 11). Each emulation run lasts 600 s (10 min). As can be seen from the CDF in Figure 12a, the 25th, 50th, 75th percentile values of the real input trace RTTs and those of the emulated path are the same while the 90th percentile RTT values are within 3.3 ms of each other. We can see that the emulation also reproduces the long-tail nature of the RTTs. We also plot the Normalized Root Mean Squared Error (NRMSE) between the real and emulated path RTTs normalized using the standard deviation of the real RTT. The NRMSE is calculated for the 25th, 50th, 75th, and 90th percentile values across 30 different emulation runs, each lasting 10 min. An NRMSE value in the range 0 to 1 is a good value where the emulation error is less than one standard deviation of the real RTT trace fed to the network emulator. As can be seen from Figure 12b all the NRMSE's

are less than 1 ms with the one for the 90th percentile being the highest, 0.62 ms. From the above results, we conclude that the network emulator can accurately emulate the cloud access times between the mobile and the cloud backend including its long tail nature.

VII. CASE STUDIES

In this section, we demonstrate the accuracy of our methodology compared to the popularly used normal distribution access time models [64]–[66]. For this purpose, we evaluate QoE metrics of real mobile applications using the developed emulation environment under our fine-tuned models and normal distribution models.

A. Instagram

In the first case study, we focus on Instagram [67], a popular social media mobile application extensively used for sharing photos and videos. We consider a hypothetical scenario in which an Instagram tester is interested in profiling the impact of cloud access time on the application level latency for the common user action of sharing a photo from the user’s device. The study is to be carried out for the LTE network of a specific MNO using a stationary device in an indoor home environment. The photo is uploaded on the cloud backend and shown to users in their feed. For this action, the application photo sharing latency is the Above The Fold Time(AFT) latency and measured as the time from when the share button is pressed by the user to the time when the posted photo’s last pixel appears on the user’s feed. In order to measure the AFT latency, we capture video of the mobile screen labeled with the time clock while performing the action and calculate the time delta using the method proposed by Brutlag et al. [68].

The measurement setup for the performance evaluation is the same as in Figure 11. We have two types of emulators, the Android mobile emulator, and the network emulator. The Android mobile emulator is deployed in our context simulation testbed [69], [70] for mobile application testing based on AWS. It has Instagram application installed on it. The mobile and network emulators are deployed on separate VM instances within the testbed (*t2.medium* type with 2 virtual CPU cores, and 4.0 GB RAM).

Now following our methodology, we collect 2500 RTT samples to the Instagram backend over the LTE network of this specific MNO using a stationary mobile device in an indoor home environment. The 2500 RTT samples are shorter than the minimum data size of 6000 and approximately an order of magnitude smaller than the largest data size of 24 000 considered in our study(see Figure 10bb). We use the *ContextPing* application running on a real Android mobile phone to collect RTT data. A configuration of sending an ICMP ping for every 500 ms is used for RTT data collection. The measurement lasts for a time duration of approximately 21 min. The task of collecting such RTT samples in the real scenarios could be crowd-sourced.

The target environment model is built by feeding the RTT samples to *ContextPerf*. *ContextPerf* pre-processes the target

environment data of 2500 RTT samples by standardizing them, and splitting them in 80:20 ratio for fine-tuning and testing, respectively. It selects a source model based on the minimum DTW measure between the source and the target environment dataset and then fine-tunes it by transferring a single layer from the source models. The SMAPE of the built target model is 14.3%. The median value of the target environment dataset is used as input to the target model to generate synthetic RTT traces from it, one step at a time for 2500 samples. These synthetic traces are then fed to the network emulator. For the performance evaluation, we also set the bandwidth and packet loss of the network in the emulation that is measured separately (also 2500 samples) using Iperf [71]. As Iperf requires access to the cloud backend, we carried out the bandwidth and packet loss measurements separately to our dummy server in AWS which was hosted in the same region as the Instagram cloud backend. For a baseline comparison, we also carry out emulation with access time traces generated from the normal distribution model. The mean and the standard deviation parameters are obtained by fitting a normal distribution to the target environment RTT data.

TABLE V: Statistical characteristics of access time traces of the LTE network — Real vs. Normal distribution vs. Synthetic

Statistic	Real LTE (ms)	Normal Distribution (ms)	Synthetic (ms)
0.01 th Percentile	36.8	33.7	35.3
50 th Percentile	43.0	43.5	43.9
99.99 th Percentile	58.1	52.8	60.1
Mean	43.4	43.5	44.5
Standard Deviation	4.2	4.1	5.2

A comparison of the statistical characteristics of the access time traces generated from our approach, the normal distribution, and the real LTE network is shown in Table V. From the results, one can see that both the synthetic traces obtained from our approach and the normal distribution traces have a similar statistical mean, median as that on the real LTE network. However, the synthetic traces perform better at extreme percentiles.

Next, we analyze the impact of these access time traces on the Instagram application AFT photo sharing latency. We wrote a simple script using Appium [72] to automate photo sharing action on Instagram. In each photo-sharing action experiment, a photo from the library is selected and shared on the profile. The screen of the emulator is recorded in the background using the Android *screencapture* tool. We repeat the experiment for 50 runs with 2 min intervals.

In order to study the impact of access time on the AFT latency, we first ran the experiments under the emulation of different fixed access times. The results (Figure 13a) show that the AFT latencies increase with an increase in the underlying access times. For the access time of 200 ms, the AFT latency can get as high as 10 s, thus leading to a significant degradation in QoE. These results indicate that access time is part of the critical path. Our findings concur with the analysis of the post

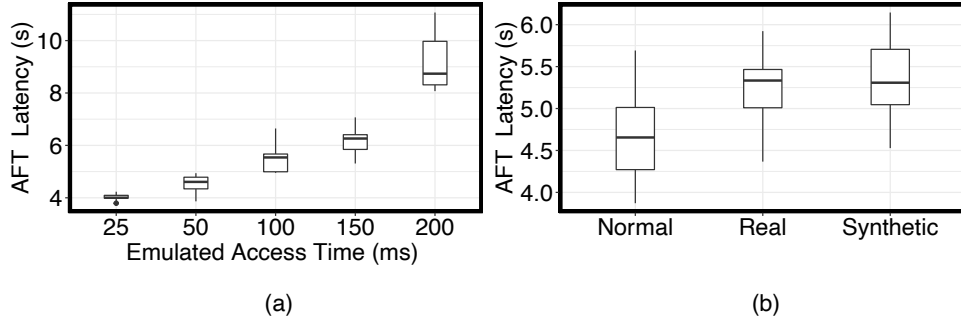


Fig. 13: Boxplot of *Instagram* AFT application photo sharing latency (seconds) measured with (a) different fixed emulated access times (b) emulation using the synthetic and normally distributed access time traces, and on an equivalent real LTE network.

sharing action of the Facebook mobile application made by Chen et al. [26].

Next, we repeat the above experiment by varying the underlying network emulation, first using our synthetic traces, and then with normally distributed traces. Finally, we also run the experiment on the real LTE network in the same home environment. Figure 13b shows the comparison of *Instagram* application AFT latencies measured under the three scenarios. The box in the figure is defined by the 25th, 50th, 75th percentiles.

In Figure 13b, one can see the variation in the measured AFT latencies across the two models and the real LTE network. The AFT latency on the real network varies from 4.3 s to 5.9 s with mean and median values being 5.2 s and 5.3 s, respectively. In the case of an emulated network with normally distributed access times, the AFT latencies are symmetrically distributed around the mean and the median. Both the mean and median values are 4.6 s. In comparison to the real LTE network, the mean and the median is lower by 13%. The maximum is 5.6 s which is lower by 8%, and the minimum is 3.8 s which is lower by 15.5%. In the case of application AFT latencies measured under the network emulation using our generated synthetic traces, both the mean and median values are 5.29 s which translates into an error of 2.0% and 0.4% compared to the real LTE network. The maximum value (6.1 s) is lower by 3.3%, while the minimum value (4.5 s) is lower by 3.6%. These error values indicate that compared to the popular normal distribution, the synthetic traces obtained using our fine-tuned model accurately estimate the AFT latencies across different quantiles.

B. Conversations

Our second case study is an Android chat messenger mobile application. *Conversations* [73] is a mobile application that uses an Extensible Messaging and Presence Protocol (XMPP) for message communication. XMPP is an XML-based communication protocol for message-oriented middleware used by many popular chat messenger applications. *Conversations* application client supports sending and receiving images, voice messages, and files with OpenPGP end-to-end message

encryption. We use an XMPP based Ejabberd [74] server as our backend for the *Conversations* application.

We suppose that an application tester is interested in analyzing the QoE metric called message delivery receipt latency for the *Conversations* application in various target environments. Message delivery receipt latency is measured as the time duration beginning from when the sender sends a message to the time when the sender receives an acknowledgment receipt for the successful delivery of that message to the recipient and displayed to the sender on the device. The delivery latencies are to be measured for a combination of different access network technologies and end-user context environment in Table VI.

The measurement setup for the performance evaluation is similar to the one used in Figure 11. The Ejabberd backend server is hosted in AWS in the EU-Ireland region. We use two separate Android emulators for a sender and a receiver with *Conversations* applications installed on them. Both Android emulators run on a separate VM instance (*t2.medium*) in our AWS based testbed. Further, to avoid the network traffic interference from the two mobile emulators, we use separate VM instances for the network emulators (also a *t2.medium*). Thus, in total, we have the following five components running on five VMs in our experimental setup: the two mobile emulators, and their two network emulator instances, and a Ejabberd backend server.

TABLE VI: Scenarios for measuring message delivery receipt latency for *Conversations* application

Scenario	Sender Environment	Receiver Environment
1	LTE Mobility Vehicle (Berlin)	WiFi Home (Berlin)
2	WiFi Home (Mumbai)	WiFi Home (Berlin)

We collect a short sample data of access times of each target environment to build its model with fine-tuning. The appropriate sample data size necessary for fine-tuning is determined by referring to the results of our earlier studies for a similar target environment (Section V-B3, Figure 10aa and Figure 10bb). From the results, a fine-tuned model with a data size of 6000 RTT samples has a SMAPE in the range of 8.0% to 21.7% for WiFi networks(Home and Office —

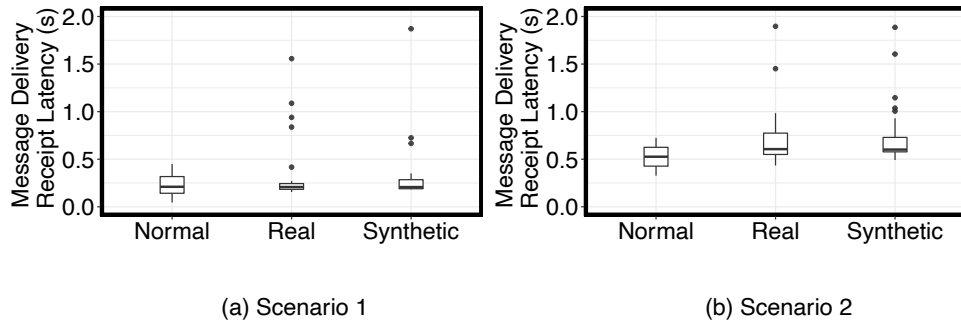


Fig. 14: Boxplot of *Conversations* application message delivery receipt latency (seconds) measured for different scenarios in Table VI with emulation using the synthetic and normally distributed access time traces, and on equivalent real networks.

Dataset 3, 4, 5, and 6) and 4.7% to 12.5% for the LTE mobility vehicle scenario (Dataset 1 and 2). On the other end, a fine-tuned model with 24000 RTT samples leads to a SMAPE in the range 3.0% to 12.7% for WiFi networks and 2.2% to 7.2% for the LTE networks. Based on these results, we decide to collect 2500 RTT samples for scenarios in Table VI. This sample size is shorter than the minimum sample size of 6000 used in our study. The measurements for the sender and the receiver environments in each scenario are carried out at the same time.

The target environment models are built by feeding the RTT samples to *ContextPerf*. The SMAPE of the obtained fine-tuned target models are 17.2% (LTE mobility vehicle — Berlin), 26.7% (WiFi Home — Berlin), and 24.5% (WiFi Home — Mumbai), 20.6% (WiFi Home — Berlin). The median value of the target environment dataset is used as input to the respective target model to generate its synthetic RTT trace for 2500 samples. The synthetic traces are fed to the network emulators together with the real measured bandwidth and packet loss traces. As in the earlier case study, the traces generated from the normal distribution model are used for baseline comparison.

The experiment to measure the message delivery receipt latency of *Conversations* application consists of sending a fixed-size 2 kB message from the sender application. The source code of the application is instrumented to log the timestamps of the message sent and acknowledgment receipt delivery events. The difference in the timestamps is calculated to obtain the message delivery receipt latency. For each of the emulation scenarios, the experiment is repeated for 50 runs. To compare the emulated message delivery receipt latencies of *Conversations* application with the real world, the experiment is repeated for 50 runs on the real access networks in the end-user context scenarios (Table VI). In order to minimize the impact of time and diurnal patterns on the network performance, these experiments were carried out sequentially immediately after the RTT samples of the target environment were collected as explained above.

Figure 14a and b show the box plots of the message delivery receipt latencies for the *Conversations* application in the two scenarios. The box in the figure is defined by the 25th and the

75th percentiles while the middle line represents the median 50th percentile. It is evident from both the figures that the delivery receipt latency distribution on the real network is positively skewed. For scenario 1 (Figure 14a) that consists of a message sender on an LTE network in a mobile vehicle, and a stationary receiver on a WiFi home network, both in the Berlin metropolitan, the mean message delivery receipt latencies are 0.28 s (real network), 0.27 s (synthetic trace), and 0.23 s (normal) while the median latencies are 0.20 s, 0.20 s, and 0.21 s, respectively. It can be seen that the mean and the median delivery receipt latencies of the *Conversations* estimated by the normal distributed access times traces and our synthetic access time traces are quite similar. And in comparison to real networks, both models accurately estimate the mean and median latencies. On the other end, the estimated maximum delivery latencies are 1.34 s (real network), 1.33 s (synthetic trace), and 0.42 s (normal), and the minimum latencies are 0.15 s, 0.18 s, and 0.05 s, respectively. The accuracy gap between the two models widens at extreme percentiles. A normally distributed access time model produces symmetric delivery receipt latencies. Furthermore, in scenario 1, it significantly underestimates the maximum and the minimum receipt delivery latencies by 72.2% and 84.4%, respectively. In scenario 2, similar behavior is observed with values underestimated by 61% and 24.4%, respectively. In contrast, our synthetic traces overestimate latencies by 20% and 21.3% (scenario 1) and 0.5% and -13.2% (scenario 2). The results show that the emulated network environment using synthetic traces obtained from fine-tuned models can accurately reproduce message delivery receipt latencies including the outlier values observed on the real networks.

C. Summary

Our case studies quantify the impact of access time model selection on the QoE metrics of two different categories of mobile applications viz. social media and chat messenger. Our results show that in both the applications, choosing the popularly used simple normal distribution access time model can provide an accurate estimation of the mean and median QoE metrics. However, the normal distribution model fares poorly at the extreme percentiles, providing conservative estimates of the QoE metrics. This can be attributed to the

fact that the underlying access times obtained from a normal distribution model are symmetric along the mean access time value. In the light of earlier studies by Amazon [10] and Google [11], these differences are quite significant. Using the popular normal distribution model for access time emulation can lead a tester to obtain overall better QoE metric estimates (message delivery receipt latency, AFT latency) and thereby falsely interpret it as superior application performance. Our case-studies also successfully demonstrate the superiority of synthetic access time traces obtained from target environment-specific fine-tuned models in mobile application testing, and the ease with which they can be realistically generated with a relatively short amount of measurement sample data.

VIII. RELATED WORK

Cloud Access Time Models — Modeling cloud access times as end-to-end delays have been extensively studied in the literature [20], [21], [75]–[80]. A time series of end-to-end delay is a sequence of data points measured at certain time intervals. Therefore, the modeling problem has been formulated as a prediction problem to estimate the next data points in the time series. We refer the readers to Yang et al. [81] for a detailed overview of various delay prediction techniques and discuss some of them briefly in the following. The widely used analytical models for end-to-end delay include Hidden Markov Models (HMM) [80] and Autoregressive (AR) models [77]. From the empirical perspective, Rao [82] presents an approach for delay prediction based on regression. On using the machine learning approach, Belhaj et al. [83] and Parlos et al. [20] have used Recurrent Neural Networks (RNN) for modeling the delay dynamics. Trevisan et al. [84] apply Kernel Density Estimation (KDE) to model mobile network characteristics. Yang et al. [21] propose a multiple model approach that predicts delay using the combination of estimates from various models treated as a bank of filters. Bui et al. [76] use wavelet transforms in combination with a recurrent multilayer perceptron neural net for long-horizon end-to-end delay prediction. There have been several measurement-based studies that have tried to characterize the end-to-end delay over different types of access networks. For instance, Manweiler et al. [85] and Huang et al. [85] have characterized the latency over 3G networks and found them to be normally distributed. All the above prediction techniques are largely data-driven, and using them for other targeted environments requires a long and laborious data collection. For instance, Belhaj et al. [83] and Parlos et al. [20], Yang, et al. [21] collect data in the order of magnitude of hours lasting an entire day. [84] ran a large-scale data collection campaign to obtain cloud access time data. This is not feasible for a tester of a single application or few applications. Unlike these studies, in our work, we focus on the problem of using a relatively shorter sample of the targeted environment in the order of magnitude of minutes to fine-tune a selected pre-trained source model.

Network Emulation Tools — Network emulation tools are also being used in analyzing the QoE of mobile applications. Network emulation has been well-studied in the literature.

Linux Traffic Control (TC) [62] is a set of utilities that enable controlling the packet traffic flow through the queueing system associated with the network interface. NetEm utility in TC has been extensively used for emulating various network conditions. Another similar tool is the network link emulator Dummynet [86] and Wide Area Network (WAN) emulator NIST Net [87]. These tools provide simple traffic shaping policies that can emulate fixed latencies as well as latencies belonging to well-known parametrized distributions like the normal distribution. The standard parametrized distributions like normal distribution are not capable of accurately emulating the time-based variability of the access times. In our work, we rely on TC for trace-driven emulation with *ContextPerf* generated synthetic access time traces. As opposed to using these tools directly for network emulation in QoE measurement, using our approach provides access network technology-specific and target environment-specific cloud access time emulation that preserves time-based variation. Furthermore, several other network emulation tools have been built based on traffic shaping algorithms viz. Augmented Traffic Control (ATC) [88] from Facebook, Network Link Conditioner [89] for MacOS, Google Chrome Devtools [90], Android Emulator [91] network emulator, etc. A feature improvement in these tools has been the addition of a network profile collection containing selected network access time traces. The traces are organized in various categories viz. Poor, Good, Lossy based on their mean and standard deviation statistics. As discussed earlier in Section I, such tools have trace profiles within a defined scope which offer limited access time variation dynamics. In contrast, the traces obtained from our access time modeling approach are more representative of a wider population of target environments.

Mobile Application QoE Measurement Tools — In this scope, there has been extensive research in building mobile application QoE measurement tools. Chen et al. [26] present a tool called QoE Doctor that uses UI automation techniques to generate user sessions to measure mobile application QoE. It also supports cross-layer analysis of mobile applications across application, transport, network, and cellular radio link layers. Another QoE analysis tool WebLAR [92] measures the web QoS metrics such as TCP connection time, and Time To First Byte (TTBF) and web QoE metrics like Above The Fold (AFT) latencies and Page Load Times (PLT). Web-PageTest [93] is another such service to measure the QoE of web applications on mobile devices. For video streaming applications like Youtube, Jimenez et al. [94] uses the network packet-level data to model the QoE of video sessions. YoMoApp by Wamser et al. [95] measures the Youtube video session QoE based on the player state/events, buffering, and video quality level data. All these tools focus on certain categories of applications. In order to measure the impact of network performance on the QoE metrics, these tools either require exposing the application to the real network conditions or use some network emulation tool, as discussed earlier. As we demonstrated in Section VII, traces generated with *ContextPerf* can be effectively used to measure the QoE metrics across

different categories of mobile applications. On the contrary, our approach complements these QoE measurement tools; it can be integrated with them to offer improved support for cloud access time emulation.

IX. FUTURE RESEARCH DIRECTION

In this section, we discuss overarching issues related to our work and future research direction.

Applicability to other network QoS metrics — While our work focuses on cloud access times, it is not the only network QoS metric that influences the application performance and its QoE. Certain categories of applications are also highly influenced by network bandwidth and packet loss. For example, video streaming applications like Youtube, audio streaming-based services like Spotify, etc. The applicability of our methodology to build bandwidth and packet loss models need to be studied and analyzed.

Widen the scope of target environments — In this work, we used a limited set of end-user contexts for building fine-tuned models. We want to evaluate *ContextPerf*'s capability under a broader range of scenarios. We are working on expanding our scope to a wider range of target environments including the effects of control plane latencies, MNOs, geographical regions, and times of the day, etc.

Applicability to next generation 5G networks and use-cases — The next generation 5G cellular networks aim to offer improved network QoS with 1000 times greater throughput improvement, 100 billion connections at a massive scale that include Machine To Machine (M2M) communication, and a close to zero latency (<1 ms) [96], [97]. With the introduction of the Enhanced Mobile Broadband (eMBB), Massive Machine Type Communications (mMTC), and Ultra Reliable and Low Latency Communications (uRLLC) services in 5G, there would be application use-cases in heterogeneous domains such as factory automation, connected vehicles, robotics, virtual reality, health care, smart city, etc. These application use-cases would have their own specific network QoS requirements. 5G stresses greater flexibility for the core network through software virtualization, thus enabling easier instantiation of the core services and simplifying radio-resource allocation without compromising on the network stability. It will also enable the different services verticals through resource sharing using network slicing [98], [99]. The impact of such network slicing decisions on the network QoS and the application QoE within the vertical would need to be studied. Understanding the QoE of the use-cases will be a key enabler of future 5G business cases. We envision an increasingly common need for target environment context driven testing in each of these service verticals where our methodology could be applied. We aim to build transfer learned 5G network QoS models, study their accuracy, and apply them to measure QoE.

***ContextPerf* automation tool release** — We plan to make the *ContextPerf* tool available to the mobile application development and the testing community to enable testers to evaluate their mobile applications QoE for a wide range of target environments. In this direction, we are working on

developing and deploying *ContextPerf* in the cloud and offer it in form of a Network Testing as a Service (NTaaS). We are targeting wider testing scenarios where testers can run cloud access time tests as a part of their periodic application release cycle.

Real world in-context trace collection — While our work improves on shortening the real-world cloud-access time traces needed to build target environment-specific models, we do recognize that sometimes access time traces might be difficult to collect. This problem can be solved to a certain extent by providing the testers with a mobile application like *ContextPing* that handles network trace collection parameterization related to granularity, scale, duration, etc. while the labeling of context data is handled by the tester. Crowdsourcing offers a promising approach to scale up trace collection. However, the collection of network trace data labeled with precise target environment context information without any user intervention comes with its own set of challenges. We leave it as a part of future work.

Applicability to other platforms – Emulators and real mobile devices — Currently, we implemented the access time emulation by integrating it in Traffic Control (TC) utility available on Linux. This limits *ContextPerf*'s ability to run seamlessly on mobile application developer and tester workstation as a part of their development workflow. Our design enables us to integrate it with other mobile emulator platforms like Android Emulator, and iOS. Furthermore, the applicability of our cloud access time emulation using a real mobile device and its trade-offs with the mobile emulator needs to be studied and verified. We also consider it a part of future work.

X. CONCLUSIONS

In this paper, we addressed the problem of generating realistic synthetic cloud access time traces for various contexts. We developed a methodology to model cloud access times with a Long Short Term Memory (LSTM) neural net using a transfer learning framework. The methodology requires a relatively short sample of cloud access time trace from a target environment to fine-tune an existing source model. To this effect, we prototyped an automation tool called *ContextPerf*, which streamlines the process of building a fine-tuned model and generating synthetic traces of context-based cloud access times from it. In real mobile application testing case-studies, we have compared the impact of different types of cloud access modeling on the application QoE. We observe that usage of the popular normal distribution access time model, as well as, of our fine-tuned model result in an accurate estimation of the mean and median QoE metrics (AFT application latency, and message delivery receipt latency). The normal distribution access time models, however, perform poorly with respect to the estimation of extreme percentiles of QoE. For example, in the case of the popular *Instagram* application, the maximum value of the AFT application latency for photo sharing action, estimated by the normal distribution model has an error of 8%, while our fine-tuned models estimate it with an error of 3.3%. Likewise, for the chat messenger application *Conversations*,

the maximum value of the QoE metric message delivery receipt latency has an estimation error of 72.2%, while our fine-tuned models estimate it with an error of only 20%. The two concrete case studies demonstrate that using our fine-tuned models result in a better assessment of QoE quantiles.

REFERENCES

- [1] J. Huang, F. Qian, A. Gerber, Z. M. Mao, S. Sen, O. Spatscheck, A close examination of performance and power characteristics of 4g lte networks, in: Proceedings of the 10th International Conference on Mobile Systems, Applications, and Services, MobiSys '12, Association for Computing Machinery, New York, NY, USA, 2012, p. 225–238. doi:10.1145/2307636.2307658.
- [2] S. Rosen, H. Luo, Q. A. Chen, Z. M. Mao, J. Hui, A. Drake, K. Lau, Discovering fine-grained rrc state dynamics and performance impacts in cellular networks, in: Proceedings of the 20th Annual International Conference on Mobile Computing and Networking, MobiCom '14, Association for Computing Machinery, New York, NY, USA, 2014, p. 177–188. doi:10.1145/2639108.2639115.
- [3] J. Erman, V. Gopalakrishnan, R. Jana, K. K. Ramakrishnan, Towards a spdy'ier mobile web?, in: Proceedings of the Ninth ACM Conference on Emerging Networking Experiments and Technologies, CoNEXT '13, Association for Computing Machinery, New York, NY, USA, 2013, p. 303–314. doi:10.1145/2535372.2535399.
- [4] S. Xu, A. Nikraves, Z. M. Mao, Leveraging context-triggered measurements to characterize LTE handover performance, in: D. R. Choffnes, M. P. Barcellos (Eds.), Passive and Active Measurement - 20th International Conference, PAM 2019, Puerto Varas, Chile, March 27–29, 2019, Proceedings, Vol. 11419 of Lecture Notes in Computer Science, Springer, 2019, pp. 3–17. doi:10.1007/978-3-030-15986-3_1.
- [5] M. Z. Shafiq, L. Ji, A. X. Liu, J. Pang, S. Venkataraman, J. Wang, A first look at cellular network performance during crowded events, SIGMETRICS Perform. Eval. Rev. 41 (1) (2013) 17–28. doi:10.1145/2494232.2465754.
- [6] J. Huang, Q. Xu, B. Tiwana, Z. M. Mao, M. Zhang, P. Bahl, Anatomizing application performance differences on smartphones, in: Proceedings of the 8th International Conference on Mobile Systems, Applications, and Services, MobiSys '10, Association for Computing Machinery, New York, NY, USA, 2010, p. 165–178. doi:10.1145/1814433.1814452.
- [7] K. Sui, M. Zhou, D. Liu, M. Ma, D. Pei, Y. Zhao, Z. Li, T. Moscibroda, Characterizing and improving wifi latency in large-scale operational networks, in: Proceedings of the 14th Annual International Conference on Mobile Systems, Applications, and Services, MobiSys '16, Association for Computing Machinery, New York, NY, USA, 2016, p. 347–360. doi:10.1145/2906388.2906393.
- [8] A. Gember, A. Akella, J. Pang, A. Varshavsky, R. Cáceres, Obtaining in-context measurements of cellular network performance, in: J. W. Byers, J. Kurose, R. Mahajan, A. C. Snoeren (Eds.), Proceedings of the 12th ACM SIGCOMM Internet Measurement Conference, IMC '12, Boston, MA, USA, November 14–16, 2012, ACM, 2012, pp. 287–300. doi:10.1145/2398776.2398807.
- [9] A. Bentaleb, B. Taani, A. C. Begen, C. Timmerer, R. Zimmermann, A survey on bitrate adaptation schemes for streaming media over http, IEEE Communications Surveys Tutorials 21 (1) (2019) 562–585. doi:10.1109/COMST.2018.2862938.
- [10] R. Kohavi, R. M. Henne, D. Sommerfield, Practical guide to controlled experiments on the web: Listen to your customers not to the hippo, in: Proceedings of the 13th ACM SIGKDD International Conference on Knowledge Discovery and Data Mining, KDD '07, Association for Computing Machinery, New York, NY, USA, 2007, p. 959–967. doi:10.1145/1281192.1281295.
- [11] Marissa Mayer at Web 2.0e, <https://www.scientiamobile.com/mobile-site-visitors-abandon-more-than-3-seconds/>, [Online; accessed 25-September-2020].
- [12] TestDevLab Blog - How To Set-up Specific Network Cconditions For Software Testing?, <https://www.testdevlab.com/blog/2017/07/how-to-set-up-specific-network-conditions-for-software-testing/>, [Online; accessed 25-September-2020].
- [13] Open Signal Maps, <http://opensignal.com>, [Online; accessed 25-September-2020].
- [14] M. E. Joorabchi, A. Mesbah, P. Kruchten, Real challenges in mobile app development, in: 2013 ACM / IEEE International Symposium on Empirical Software Engineering and Measurement, 2013, pp. 15–24. doi:10.1109/ESEM.2013.9.
- [15] B. D. Noble, M. Satyanarayanan, G. T. Nguyen, R. H. Katz, Trace-based mobile network emulation, in: Proceedings of the ACM SIGCOMM '97 Conference on Applications, Technologies, Architectures, and Protocols for Computer Communication, SIGCOMM '97, ACM, New York, NY, USA, 1997, pp. 51–61. doi:10.1145/263105.263140.
- [16] Testing on Emulators vs Simulators vs Real devices, <https://www.browserstack.com/guide/testing-on-emulators-simulators-real-devices-comparison>, [Online; accessed 25-September-2020].
- [17] U. Goel, M. Steiner, M. P. Wittie, S. Ludin, M. Flack, Domain-sharding for faster HTTP/2 in lossy cellular networks, CoRR abs/1707.05836. arXiv:1707.05836.
- [18] M. Hirth, T. Hößfeld, M. Mellia, C. Schwartz, F. Lehrieder, Crowd-sourced network measurements: Benefits and best practices, Computer Networks 90 (2015) 85 – 98, crowdsourcing. doi:https://doi.org/10.1016/j.comnet.2015.07.003.
- [19] U. Goel, M. P. Wittie, K. C. Claffy, A. Le, Survey of end-to-end mobile network measurement testbeds, tools, and services, IEEE Communications Surveys Tutorials 18 (1) (2016) 105–123. doi:10.1109/COMST.2015.2485979.
- [20] A. G. Parlos, Identification of the internet end-to-end delay dynamics using multi-step neuro-predictors, in: Proceedings of the 2002 International Joint Conference on Neural Networks. IJCNN'02 (Cat. No.02CH37290), Vol. 3, 2002, pp. 2460–2465 vol.3. doi:10.1109/IJCNN.2002.1007528.
- [21] M. Yang, J. Ru, X. R. Li, H. Chen, A. Bashi, Predicting internet end-to-end delay: A multiple-model approach, in: Proceedings IEEE INFOCOM 2006. 25TH IEEE International Conference on Computer Communications, 2006, pp. 1–5. doi:10.1109/INFOCOM.2006.345.
- [22] X. S. Wang, A. Balasubramanian, A. Krishnamurthy, D. Wetherall, Demystifying page load performance with wprof, in: 10th USENIX Symposium on Networked Systems Design and Implementation (NSDI 13), USENIX Association, Lombard, IL, 2013, pp. 473–485.
- [23] More Bandwidth Doesn't Matter (Much), <https://www.belshe.com/2010/05/24/more-bandwidth-doesnt-matter-much/>, [Online; accessed 25-September-2020].
- [24] J. Nejadi, A. Balasubramanian, An in-depth study of mobile browser performance, in: Proceedings of the 25th International Conference on World Wide Web, WWW '16, International World Wide Web Conferences Steering Committee, Republic and Canton of Geneva, CHE, 2016, p. 1305–1315. doi:10.1145/2872427.2883014.
- [25] I. Grigorik, High Performance Browser Networking: What Every Web Developer Should Know about Networking and Web Performance, 1st Edition, O'Reilly Media, 2013.
- [26] Q. A. Chen, H. Luo, S. Rosen, Z. M. Mao, K. Iyer, J. Hui, K. Sontineni, K. Lau, Qoe doctor: Diagnosing mobile app qoe with automated ui control and cross-layer analysis, in: Proceedings of the 2014 Conference on Internet Measurement Conference, IMC '14, Association for Computing Machinery, New York, NY, USA, 2014, p. 151–164. doi:10.1145/2663716.2663726.
- [27] A. Zuniga, H. Flores, E. Lagerspetz, P. Nurmi, S. Tarkoma, P. Hui, J. Manner, Tortoise or hare? quantifying the effects of performance on mobile app retention, in: The World Wide Web Conference, WWW '19, Association for Computing Machinery, New York, NY, USA, 2019, p. 2517–2528. doi:10.1145/3308558.3313428.
- [28] E. M. Bishop, Hypertext Transfer Protocol Version 3 (HTTP/3), Tech. Rep. 1654 (February 2021). URL <https://tools.ietf.org/html/draft-ietf-quic-http-34>
- [29] P. Megyesi, Z. Krämer, S. Molnár, How quick is quic?, in: 2016 IEEE International Conference on Communications (ICC), 2016, pp. 1–6. doi:10.1109/ICC.2016.7510788.
- [30] S. Cook, B. Mathieu, P. Truong, I. Hamchaoui, Quic: Better for what and for whom?, in: 2017 IEEE International Conference on Communications (ICC), 2017, pp. 1–6. doi:10.1109/ICC.2017.7997281.
- [31] A. M. Kakhki, S. Jero, D. Choffnes, C. Nita-Rotaru, A. Mislove, Taking a long look at quic: An approach for rigorous evaluation of rapidly evolving transport protocols, in: Proceedings of the 2017 Internet Measurement Conference, IMC '17, Association for Computing Machinery,

- New York, NY, USA, 2017, p. 290–303. doi:10.1145/3131365.3131368.
- [32] A. Nikraves, D. R. Choffnes, E. Katz-Bassett, Z. M. Mao, M. Welsh, Mobile network performance from user devices: A longitudinal, multidimensional analysis, in: *Passive and Active Measurement - 15th International Conference, PAM 2014, Los Angeles, CA, USA, March 10-11, 2014, Proceedings, 2014*, pp. 12–22.
 - [33] K.-T. Chen, C.-Y. Huang, P. Huang, C.-L. Lei, Quantifying skype user satisfaction, in: *Proceedings of the 2006 Conference on Applications, Technologies, Architectures, and Protocols for Computer Communications, SIGCOMM '06, Association for Computing Machinery, New York, NY, USA, 2006*, p. 399–410. doi:10.1145/1159913.1159959.
 - [34] Quality of Service Design Overview, <https://www.ciscopress.com/articles/article.asp?p=357102>, [Online; accessed 25-September-2020].
 - [35] S. Wang, S. Dey, Modeling and characterizing user experience in a cloud server based mobile gaming approach, in: *GLOBECOM 2009 - 2009 IEEE Global Telecommunications Conference, 2009*, pp. 1–7. doi:10.1109/GLOCOM.2009.5425784.
 - [36] L. Pantel, L. C. Wolf, On the impact of delay on real-time multiplayer games, in: *Proceedings of the 12th International Workshop on Network and Operating Systems Support for Digital Audio and Video, NOSSDAV '02, Association for Computing Machinery, New York, NY, USA, 2002*, p. 23–29. doi:10.1145/507670.507674.
 - [37] M. Claypool, K. Claypool, Latency and player actions in online games, *Commun. ACM* 49 (11) (2006) 40–45. doi:10.1145/1167838.1167860.
 - [38] N. Sheldon, E. Girard, S. Borg, M. Claypool, E. Agu, The effect of latency on user performance in warcraft iii, in: *Proceedings of the 2nd Workshop on Network and System Support for Games, NetGames '03, Association for Computing Machinery, New York, NY, USA, 2003*, p. 3–14. doi:10.1145/963900.963901.
 - [39] S. Hochreiter, J. Schmidhuber, Long short-term memory, *Neural Comput.* 9 (8) (1997) 1735–1780. doi:10.1162/neco.1997.9.8.1735.
 - [40] A. Graves, Generating sequences with recurrent neural networks, *CoRR* abs/1308.0850. arXiv:1308.0850.
 - [41] R. Pascanu, T. Mikolov, Y. Bengio, On the difficulty of training recurrent neural networks, in: *Proceedings of the 30th International Conference on International Conference on Machine Learning - Volume 28, ICML '13, JMLR.org, 2013*, pp. III–1310–III–1318.
 - [42] I. Sutskever, O. Vinyals, Q. V. Le, Sequence to sequence learning with neural networks, in: *Proceedings of the 27th International Conference on Neural Information Processing Systems, NIPS'14, MIT Press, Cambridge, MA, USA, 2014*, pp. 3104–3112.
 - [43] K. Weiss, T. M. Khoshgoftaar, D. Wang, A survey of transfer learning, *Journal of Big Data* 3 (1) (2016) 9. doi:10.1186/s40537-016-0043-6.
 - [44] A. Krizhevsky, I. Sutskever, G. E. Hinton, Imagenet classification with deep convolutional neural networks, *Commun. ACM* 60 (6) (2017) 84–90. doi:10.1145/3065386.
 - [45] Z. Chen, Y. Yang, in: *Assessing Forecast Accuracy Measures, Technical Report, Department of Statistics and Statistical Laboratory, Iowa State University: Ames, IA, USA, 2004*.
 - [46] J. Armstrong, F. Collopy, Error measures for generalizing about forecasting methods: Empirical comparisons, *International Journal of Forecasting* 8 (1) (1992) 69–80. doi:https://doi.org/10.1016/0169-2070(92)90008-W.
 - [47] S. Makridakis, Accuracy measures: theoretical and practical concerns, *International Journal of Forecasting* 9 (4) (1993) 527–529. doi:https://doi.org/10.1016/0169-2070(93)90079-3.
 - [48] P. Goodwin, R. Lawton, On the asymmetry of the symmetric mape, *International Journal of Forecasting* 15 (4) (1999) 405–408. doi:https://doi.org/10.1016/S0169-2070(99)00007-2.
 - [49] L. Nikolay, Y. Jason, E. L. Li, S. Slawek, Time-series extreme event forecasting with neural networks at uber, in: *International Conference on Machine Learning Time Series Workshop, 2017*.
 - [50] L. Nikolay, Y. Jiafan, R. Rajagopal, Reconstruction and regression loss for time-series transfer learning, in: *4th Workshop On Mining and Learning From Time Series, KDD, London, UK, 2018*.
 - [51] N. Srivastava, G. E. Hinton, A. Krizhevsky, I. Sutskever, R. Salakhutdinov, Dropout: a simple way to prevent neural networks from overfitting, *J. Mach. Learn. Res.* 15 (1) (2014) 1929–1958.
 - [52] D. Clevert, T. Unterthiner, S. Hochreiter, Fast and accurate deep network learning by exponential linear units (elus), in: Y. Bengio, Y. LeCun (Eds.), *4th International Conference on Learning Representations, ICLR 2016, San Juan, Puerto Rico, May 2-4, 2016, Conference Track Proceedings, 2016*.
 - [53] J. Lee, K. Shridhar, H. Hayashi, B. K. Iwana, S. Kang, S. Uchida, Probat: A probabilistic activation function for deep neural networks, *CoRR* abs/1905.10761. arXiv:1905.10761.
 - [54] D. P. Kingma, J. Ba, Adam: A method for stochastic optimization, in: Y. Bengio, Y. LeCun (Eds.), *3rd International Conference on Learning Representations, ICLR 2015, San Diego, CA, USA, May 7-9, 2015, Conference Track Proceedings, 2015*.
 - [55] Keras: The Python Deep Learning Library, <https://keras.io/>, [Online; accessed 25-September-2020].
 - [56] Z. Wang, Z. Dai, B. Póczos, J. G. Carbonell, Characterizing and avoiding negative transfer, in: *IEEE Conference on Computer Vision and Pattern Recognition, CVPR 2019, Long Beach, CA, USA, June 16-20, 2019, Computer Vision Foundation / IEEE, 2019*, pp. 11293–11302. doi:10.1109/CVPR.2019.01155.
 - [57] H. I. Fawaz, G. Forestier, J. Weber, L. Idoumghar, P. Muller, Transfer learning for time series classification, *CoRR* abs/1811.01533. arXiv:1811.01533.
 - [58] J. Yosinski, J. Clune, Y. Bengio, H. Lipson, How transferable are features in deep neural networks?, in: Z. Ghahramani, M. Welling, C. Cortes, N. D. Lawrence, K. Q. Weinberger (Eds.), *Advances in Neural Information Processing Systems 27: Annual Conference on Neural Information Processing Systems 2014, December 8-13 2014, Montreal, Quebec, Canada, 2014*, pp. 3320–3328.
 - [59] Google Cloud Machine Types, <https://cloud.google.com/compute/docs/machine-types>, [Online; accessed 25-September-2020].
 - [60] U. Goel, M. Steiner, M. P. Wittie, S. Ludin, M. Flack, cell-emulation-util, <https://github.com/akamai/cell-emulation-util>, [Online; accessed 25-September-2020].
 - [61] Herve Eyche, iptables(8) - Linux man page, <https://linux.die.net/man/8/iptables>, [Online; accessed 25-September-2020].
 - [62] Bert Hubert, tc(8) - Linux man page, <https://linux.die.net/man/8/tc>, [Online; accessed 25-September-2020].
 - [63] Terraform, <https://www.terraform.io/>, [Online; accessed 25-September-2020].
 - [64] J. Manweiler, S. Agarwal, M. Zhang, R. R. Choudhury, P. Bahl, Switchboard: a matchmaking system for multiplayer mobile games, in: *Proceedings of the 9th International Conference on Mobile Systems, Applications, and Services (MobiSys 2011), Bethesda, MD, USA, June 28 - July 01, 2011, 2011*, pp. 71–84. doi:10.1145/1999995.2000003.
 - [65] J. Huang, Q. Xu, B. Tiwana, Z. M. Mao, M. Zhang, P. Bahl, Anatomizing application performance differences on smartphones, in: *Proceedings of the 8th International Conference on Mobile Systems, Applications, and Services, MobiSys '10, Association for Computing Machinery, New York, NY, USA, 2010*, p. 165–178. doi:10.1145/1814433.1814452.
 - [66] R. Mittal, A. Kansal, R. Chandra, Empowering developers to estimate app energy consumption, in: *Proceedings of the 18th Annual International Conference on Mobile Computing and Networking, Mobicom '12, Association for Computing Machinery, New York, NY, USA, 2012*, p. 317–328. doi:10.1145/2348543.2348583.
 - [67] Instagram, <https://www.instagram.com/>, [Online; accessed 25-September-2020].
 - [68] Above the fold time: Measuring web page performance visually, http://cdn.oreillystatic.com/en/assets/1/event/62/Above%20the%20Fold%20Time_%20Measuring%20Web%20Page%20Performance%20Visually%20Presentation.pdf, [Online; accessed 25-September-2020].
 - [69] M. R. Rege, V. Handziski, A. Wolisz, Realistic context generation for mobile app testing and performance evaluation, in: *2017 IEEE International Conference on Pervasive Computing and Communications, PerCom 2017, Kona, Big Island, HI, USA, March 13-17, 2017, 2017*, pp. 297–308.
 - [70] M. R. Rege, V. Handziski, A. Wolisz, Crowdmeter: An emulation platform for performance evaluation of crowd-sensing applications, in: *Proceedings of the 2013 ACM Conference on Pervasive and Ubiquitous Computing Adjunct Publication, UbiComp '13 Adjunct, Association for Computing Machinery, New York, NY, USA, 2013*, p. 1111–1122. doi:10.1145/2494091.2499578.

- [71] iperf3: A tcp, udp, and sctp network bandwidth measurement tool, <https://github.com/esnet/iperf>, [Online; accessed 25-September-2020].
- [72] Appium - Automation for Apps, <http://appium.io/>, [Online; accessed 25-September-2020].
- [73] Conversations: the very last word in instant messaging, <https://github.com/siacs/Conversations>, [Online; accessed 25-September-2020].
- [74] Ejabberd: Robust, Scalable and Extensible Realtime Server using XMPP, MQTT and SIP, <https://www.ejabberd.im/>, [Online; accessed 25-September-2020].
- [75] Zhihao Guo, B. Malakooti, Delay prediction for intelligent routing in wireless networks using neural networks, in: 2006 IEEE International Conference on Networking, Sensing and Control, 2006, pp. 625–630. doi:10.1109/ICNSC.2006.1673218.
- [76] V. Bui, W. Zhu, A. Pescapé, A. Botta, Long horizon end-to-end delay forecasts: A multi-step-ahead hybrid approach, in: 2007 12th IEEE Symposium on Computers and Communications, 2007, pp. 825–832. doi:10.1109/ISCC.2007.4381513.
- [77] H. Ohsaki, M. Murata, H. Miyahara, Modeling end-to-end packet delay dynamics of the internet using system identification, in: J. M. de Souza, N. L. da Fonseca, E. A. de Souza e Silva (Eds.), *Teletraffic Engineering in the Internet Era*, Vol. 4 of *Teletraffic Science and Engineering*, Elsevier, 2001, pp. 1027 – 1038. doi:[https://doi.org/10.1016/S1388-3437\(01\)80189-X](https://doi.org/10.1016/S1388-3437(01)80189-X).
- [78] V. Paxson, End-to-end internet packet dynamics, *SIGCOMM Comput. Commun. Rev.* 27 (4) (1997) 139–152. doi:10.1145/263109.263155.
- [79] P. Sanaga, J. Duerig, R. Ricci, J. Lepreau, Modeling and emulation of internet paths, in: *Proceedings of the 6th USENIX Symposium on Networked Systems Design and Implementation, NSDI'09*, USENIX Association, Berkeley, CA, USA, 2009, pp. 199–212.
- [80] M. Mouchet, S. Vaton, T. Chonavel, Statistical characterization of round-trip times with nonparametric hidden markov models, in: 2019 IFIP/IEEE Symposium on Integrated Network and Service Management (IM), 2019, pp. 43–48.
- [81] Ming Yang, X. R. Li, Huimin Chen, N. S. V. Rao, Predicting internet end-to-end delay: an overview, in: *Thirty-Sixth Southeastern Symposium on System Theory*, 2004. *Proceedings of the*, 2004, pp. 210–214. doi:10.1109/SSST.2004.1295650.
- [82] N. S. V. Rao, Overlay networks of in situ instruments for probabilistic guarantees on message delays in wide-area networks, *IEEE Journal on Selected Areas in Communications* 22 (1) (2004) 79–90. doi:10.1109/JSAC.2003.818797.
- [83] S. Belhaj, M. Tagina, Modeling and prediction of the internet end-to-end delay using recurrent neural networks, *Journal of Networks* 4. doi:10.4304/jnw.4.6.528–535.
- [84] M. Trevisan, A. Safari Khatouni, D. Giordano, Errant: Realistic emulation of radio access networks, *Computer Networks* 176 (2020) 107289. doi:<https://doi.org/10.1016/j.comnet.2020.107289>.
- [85] J. Manweiler, S. Agarwal, M. Zhang, R. Roy Choudhury, P. Bahl, Switchboard: A matchmaking system for multiplayer mobile games, in: *Proceedings of the 9th International Conference on Mobile Systems, Applications, and Services, MobiSys '11*, Association for Computing Machinery, New York, NY, USA, 2011, p. 71–84. doi:10.1145/1999995.2000003.
- [86] L. Rizzo, Dummynet: A simple approach to the evaluation of network protocols, *SIGCOMM Comput. Commun. Rev.* 27 (1) (1997) 31–41. doi:10.1145/251007.251012.
- [87] M. Carson, D. Santay, Nist net: A linux-based network emulation tool, *SIGCOMM Comput. Commun. Rev.* 33 (3) (2003) 111–126. doi:10.1145/956993.957007.
- [88] Augmented Traffic Control, <https://github.com/facebookarchive/augmented-traffic-control>, [Online; accessed 25-September-2020].
- [89] Network Link Conditioner, <https://nshipster.com/network-link-conditioner/>, [Online; accessed 25-September-2020].
- [90] Simulate Mobile Devices with Device Mode in Chrome Devtools, <https://developers.google.com/web/tools/chrome-devtools/device-mode>, [Online; accessed 25-September-2020].
- [91] Android Emulator, <http://developer.android.com/tools/help/emulator.html>, [Online; accessed 25-September-2020].
- [92] A. S. Asrese, E. A. Walelgne, V. Bajpai, A. Lutu, Ö. Alay, J. Ott, Measuring web quality of experience in cellular networks, in: D. R. Choffnes, M. P. Barcellos (Eds.), *Passive and Active Measurement - 20th International Conference, PAM 2019, Puerto Varas, Chile, March 27-29, 2019, Proceedings*, Vol. 11419 of *Lecture Notes in Computer Science*, Springer, 2019, pp. 18–33. doi:10.1007/978-3-030-15986-3_2.
- [93] WebPageTest, <https://www.webpagetest.org/>, [Online; accessed 25-September-2020].
- [94] L. R. Jiménez, M. Solera, M. Toril, A network-layer qoe model for youtube live in wireless networks, *IEEE Access* 7 (2019) 70237–70252. doi:10.1109/ACCESS.2019.2918433.
- [95] F. Wamser, M. Seufert, P. Casas, R. Irmer, P. Tran-Gia, R. Schatz, Yomoapp: A tool for analyzing qoe of youtube http adaptive streaming in mobile networks, in: *2015 European Conference on Networks and Communications (EuCNC)*, 2015, pp. 239–243. doi:10.1109/EuCNC.2015.7194076.
- [96] M. Agiwal, A. Roy, N. Saxena, Next generation 5g wireless networks: A comprehensive survey, *IEEE Commun. Surv. Tutorials* 18 (3) (2016) 1617–1655. doi:10.1109/COMST.2016.2532458.
- [97] A. Gupta, R. K. Jha, A survey of 5g network: Architecture and emerging technologies, *IEEE Access* 3 (2015) 1206–1232. doi:10.1109/ACCESS.2015.2461602.
- [98] F. Z. Yousaf, M. Gramaglia, V. Friderikos, B. Gajic, D. von Hugo, B. Sayadi, V. Sciancalepore, M. R. Crippa, Network slicing with flexible mobility and qos/qoe support for 5g networks, in: *2017 IEEE International Conference on Communications Workshops (ICC Workshops)*, 2017, pp. 1195–1201. doi:10.1109/ICCW.2017.7962821.
- [99] X. Foukas, G. Patounas, A. Elmokashfi, M. K. Marina, Network slicing in 5g: Survey and challenges, *IEEE Communications Magazine* 55 (5) (2017) 94–100. doi:10.1109/MCOM.2017.1600951.